

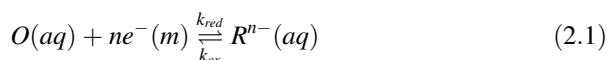
Chapter 2

Interpreting Electrochemistry

This chapter introduces readers to the important aspects of electrochemistry which allow a greater understanding and appreciation of the subject, which can then be applied in later chapters where graphene is utilised as an electrode material.

2.1 Introduction

If you have studied science at undergraduate level you will be familiar with Faraday's law and electrode potentials, and appreciate that electrochemical reactions involve charged species whose energy depends on the potential of the phase that such species are contained within. Consider the following simple reversible redox reaction:



where O and R are the oxidised and reduced forms of a redox couple in an aqueous media. The electrochemical process as expressed in Eq. (2.1) involves the transfer of charge across the interfacial region of a metallic electrode, termed (m) to indicate the source of electrons, and a solution phase (aq) species. The electrochemical reaction described in Eq. (2.1) only proceeds once a suitable electrode is placed into the solution phase, which acts as a source or sink of electrons. It is important to realise that this reaction involves the transfer of charged species, viz electrons, between the electrode surface (m), and the solution phase species (aq), hence the electrode reaction is an interfacial process. As the electron transfer moves towards equilibrium a net charge separation must develop between the electrode and the solution which creates a potential difference at the solution | electrode interface, which is expressed as ϕ_s and ϕ_m respectively, such that the potential drop across the interface is thus:

$$\Delta\phi = \phi_m - \phi_s \quad (2.2)$$

In order to measure such a value a complete conducting circuit is required. However, if another electrode is placed into the solution then you have two electrodes, both monitoring the change of the potential difference at the two electrode | solution interfaces, resulting in meaningless information. The solution is to use one electrode | solution interface and a reference electrode which maintains a fixed potential difference, which leads to the following being realised:

$$E = (\phi_m - \phi_s) + X \quad (2.3)$$

where E is the potential difference being measured, the term $E = (\phi_m - \phi_s) + X$ refers to the electrode of interest and X is the role of the reference electrode, which is constant. Such measurements are undertaken at equilibrium such that no current is drawn through the cell. The potential E reaches a steady value, E_e which now depends on the relative concentrations of O and R , which can be expressed as:

$$E_e = \Delta\phi_{m/s}(O/R) - \Delta\phi_{m/s}(X) = \Delta\phi_{m/s}(O/R) - 0 \quad (2.4)$$

where X is a reference electrode such as the Standard Hydrogen Electrode (SHE) or the more commonly utilised Saturated Calomel Electrode (SCE). Conventionally the SHE is defined as exhibiting a potential of zero, allowing one to report the potential of half-cells such as the O/R couple, relative to the SHE. For the process defined in Eq. (2.1), the *Nernst equation* is given by:

$$E_e = E_f^0(O/R) + \left(\frac{RT}{nF}\right) \ln\left(\frac{[O]}{[R]}\right) \quad (2.5)$$

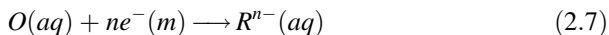
for the potential established at the electrode under equilibrium, where E_e is the equilibrium potential of the formal potential E_f^0 and the concentrations of the species O and R at the electrode surface, which, under conditions of equilibrium, are the same as their bulk solution values. Such potential determining equilibrium should be familiar from general undergraduate science classes. Above, R is the universal gas constant ($8.314 \text{ J K}^{-1} \text{ mol}^{-1}$), T is the temperature (in Kelvin), n is the number of electrons transferred in the reaction and F is the Faraday constant ($96,485.33 \text{ C mol}^{-1}$). Note that in Eq. (2.5) the formal potential is defined as:

$$E_f^0 = E^0(O/R) + \left(\frac{RT}{nF}\right) \ln\left(\frac{\gamma_O^v}{\gamma_R^v}\right) \quad (2.6)$$

where E^0 is the standard electrode potential and γ is the relevant activity coefficients. The formal potentials depend on temperature and pressure, as do the standard potentials, but will also have a dependence on electrolyte concentrations, not only of the species involved in the potential determining equilibrium but also on other electrolytes that will be present in the solution since these influence ion activities. The formal potential loses the thermodynamic generality of the standard potentials which are only applicable under specific conditions but enables experimentalists to proceed with meaningful voltammetric measurements.

Equilibrium electrochemistry, viz equilibrium electrochemical measurements, while being of fundamental importance since it allows thermodynamic parameters to be readily obtained (such as reaction free energies, entropies, equilibrium constants and solution pH), it is a rather dry subject and not as exciting as dynamic electrochemistry which is the main thrust of electrochemistry that is used commercially in numerous areas, such as in sensing and energy storage/generation.

If we depart from equilibrium electrochemistry to that of dynamic electrochemistry, consider the following electrochemical process:



at an electrode which is brought about through the application of a suitability negative potential to the electrode. Note that a second electrode will be needed somewhere in the solution to facilitate the passage of the required electrical current through the solution and a reference electrode will also be required as identified above. The process, as described in Fig. 2.1 occurs in the following general steps. First, the reactant diffuses from the bulk solution to the electrode interface, termed mass transport. Next, a potential is applied into the cell which is different to E_e , the potential difference induces the exchange of electrons between the electrode surface and the species in solution and as such, electrolysis occurs where the magnitude of the current, i , is related to the flux of the species in solution, j , by the following:

$$i = nAFj \quad (2.8)$$

where F is the Faraday constant, n is the number of electrons per molecule involved in the electrochemical process and A is the electrode area. The electron transfer process between the electrode and the $O(aq)$ species takes place via quantum mechanical tunnelling between the electrode and reactant close to the electrode, typically *ca.* 10–20 Å as the rate of tunnelling falls off strongly with separation since it requires overlap of quantum mechanical wave-functions which describes the electron in the electrode and the electroactive species. Note that the above process is complicated by the reactivity of the electro-active species, the nature (type, geometry) of the electrode surface, the applied voltage and the structure of the interfacial region over which the electron transfer process occurs.

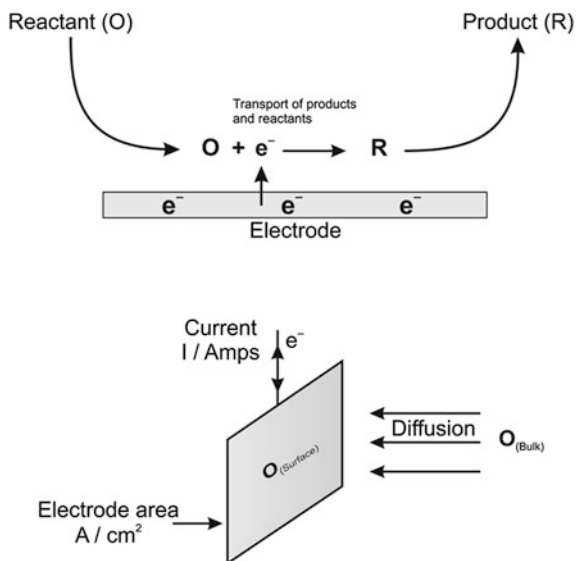
In Eq. (2.8) the units of flux are: $\text{moles cm}^{-2} \text{ s}^{-1}$, which effectively reflects the quantity of material reaching the electrode surface per second. Akin to homogeneous kinetics, the rate law can be described by:

$$j = k(n)[\text{Reactant}]_0 \quad (2.9)$$

Where $k(n)$ is the n th order rate constant for the electron transfer reaction and $[\text{Reactant}]_0$ is the concentration of the electro-active reactant species at the electrode surface (and not in the bulk solution): when $n = 1$, as commonly encountered, corresponding to a 1st order heterogeneous reaction, the units are cm s^{-1} .

The most common configuration for running dynamic electrochemical experiments involves the use of three electrodes, the working electrode, a counter

Fig. 2.1 Schematic representation of a simple electrode reaction



(auxiliary) electrode and a reference electrode, all connected to a commercially available potentiostat which allows the potential difference between the reference and working electrode to be controlled with minimal interference from ohmic (IR) drop. The current flowing through the reference electrode is minimised avoiding polarisation of the reference electrode and this keeps the applied potential between the working and reference electrode stable. Shown in Fig. 2.2 is a typical experimental set-up where the three electrode system is being utilised. The reference electrode can be a Ag/AgCl or a SCE which can either be commercially obtained or fabricated within the laboratory. The counter electrode should be a non-reactive high surface area electrode such as platinum or carbon and the working electrode can be a plethora of configurations and compositions, indeed, researchers are trying to utilise graphene as an electrode material, which we will learn about in the subsequent chapters of this *handbook*.

If we concern ourselves with only the working electrode since it is where all the significant processes occur, a general overview of an electrode reaction is depicted in Fig. 2.3 which builds on that shown in Fig. 2.1. This general electrochemical process shows that the observed electrode current is dependent upon mass transport which usually occurs in series with other processes, such as chemical reactions, adsorption/desorption and also the heterogeneous rate constant for the electron transfer reaction. The working electrode is immersed into an electrolyte usually containing the electroactive species under investigation and a supporting electrolyte salt to achieve the required conductivity and to minimise the IR drop. The electric double layer at the working electrode occurs over a distance of *ca.* 1 nm. Figure 2.4 shows a schematic representation of the composition of the solution phase close to the (working) electrode surface where the compact layer is also

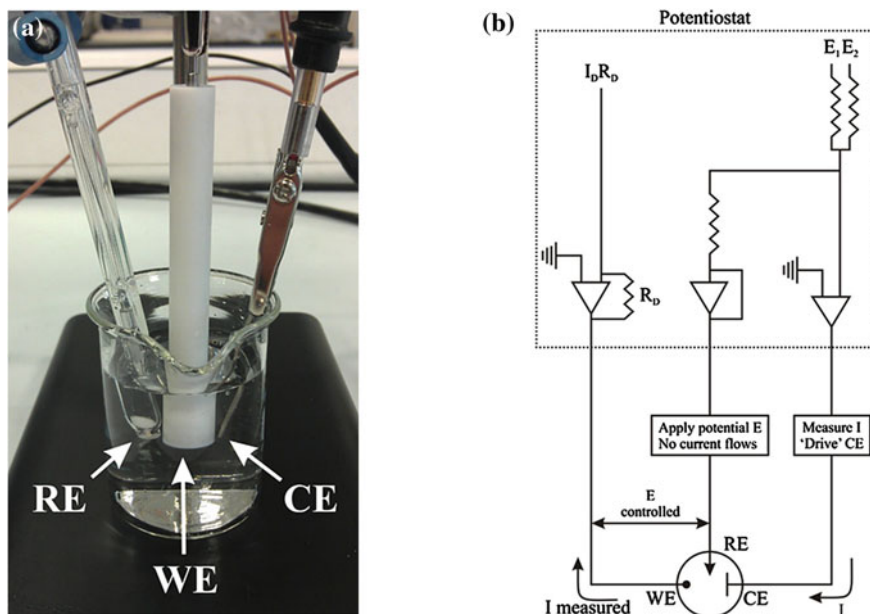
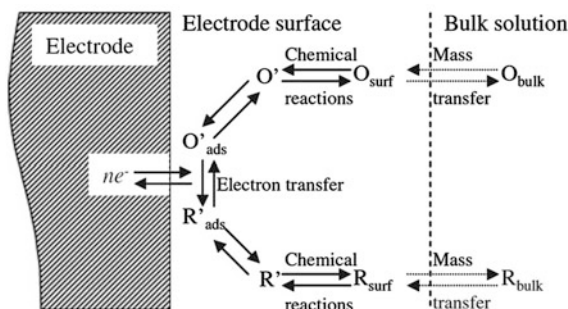


Fig. 2.2 **a** A typical experimental set-up showing the reference electrode (*RE*, saturated calomel electrode), the working electrode (*WE*) and the counter electrode (*CE*, a platinum rod) immersed into an electrolyte solution. **b** A simple electronic scheme equivalent to the electrochemical cell. A potentiostat is required for running electrochemical experiments. Note all the resistances are equal except R_D which is variable

Fig. 2.3 The general electrochemical reaction pathway



termed the “inner Helmholtz” layer which is closest to the surface in which the distribution of charge, and hence potential, changes linearly with the distance from the electrode surface and the diffuse layer, known as the “Gouy-Chapman” layer, in which the potential changes exponentially. Also shown in Fig. 2.4 is a zoomed in perspective of the compact layer showing the Inner and Outer Helmholtz Plane (IHP and OHP) where specifically adsorbed anions and solvated cations can reside.

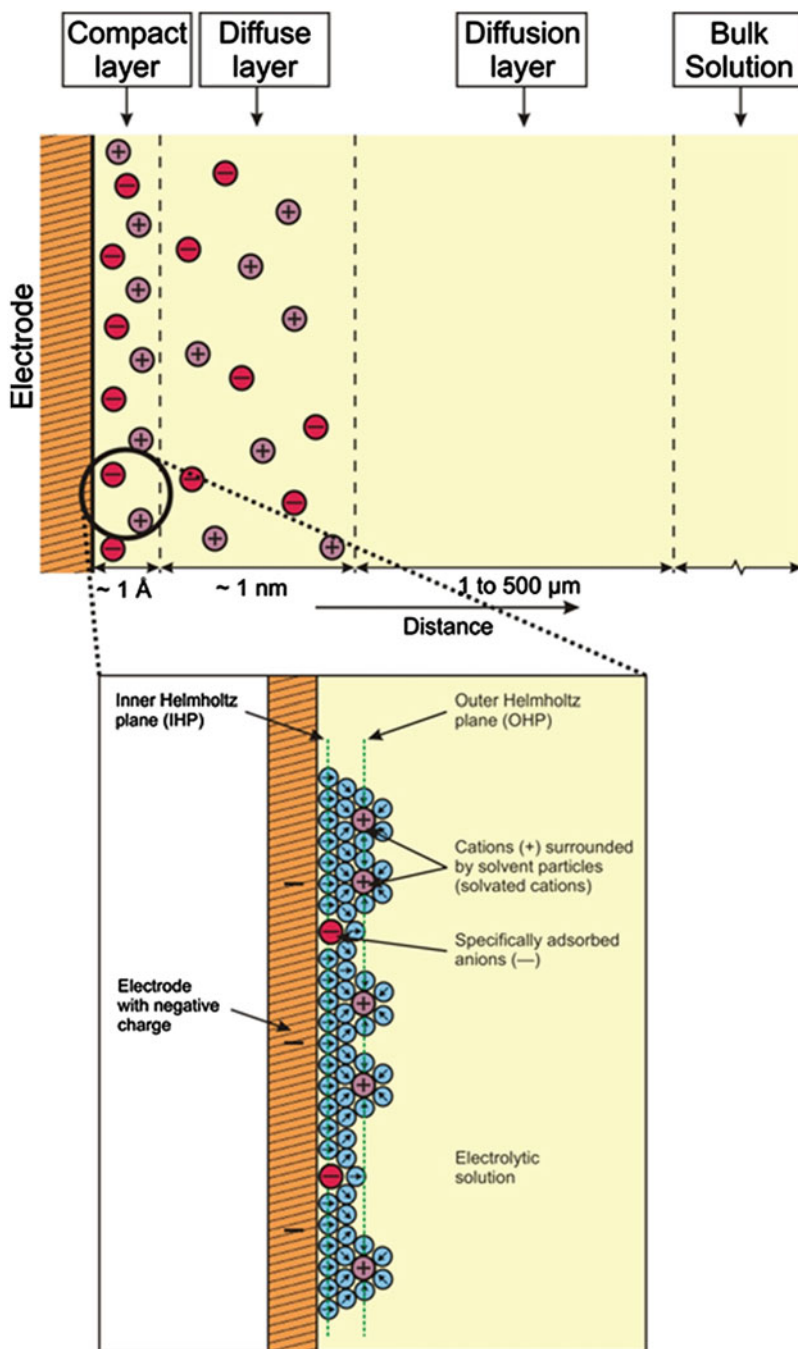


Fig. 2.4 Schematic representation of the composition of the electrode | solution interface (not to scale)

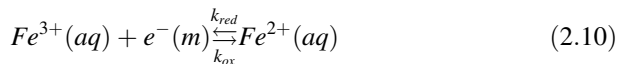
Under typical experimental conditions, the magnitude of the diffusion layer is several orders of magnitude larger than the diffuse layer. In dynamic electrochemistry the potential is always being changed and hence the surface orientation will change and a concentration perturbation travels away from the electrode surface into the solution, where the diffusion layer (δ) is related to the diffusion coefficient of the electroactive species being perturbed as a function of time (t). We return to the diffusion layer when discussing cyclic voltammetry.

As discussed above with reference to Fig. 2.1, the application of a voltage is key for electrochemical reactions to proceed. The application of a potential, that is, a voltage, $V = \text{Joule/Coulombs}$, such that the voltage is simply the energy (Joule) required to move charge (Coulomb). The application of such a voltage supplies electrical energy and can be thought of as an electrochemical ‘pressure’.

The electronic structure of a metal involves electronic conduction bands in which electrons are free to move throughout the metal, which binds the (metal) cations together. The energy levels in these bands form an effective continuum of levels, which are filled-up to an energy maximum (Fermi level). Such levels can be altered by supplying electrical energy in the form of applying or driving a voltage, as shown in Fig. 2.5a. In Fig. 2.5b (left image), the Fermi level energy is lower than that of the Lowest Unoccupied Molecular Orbital (LUMO) of the reactant and as such it is *thermodynamically unfavourable* for an electron to jump/transfer from the electrode to the molecule. However, as shown in Fig. 2.5b (right image), when the Fermi level of the electrode is above the LUMO of the reactant it is then *thermodynamically favourable* for the electron transfer process to occur, that is, the electrochemical reduction of the reactant can proceed. This concept is explored further in Sect. 2.2 as the process depends on the kinetics of the electrochemical transfer reaction.

2.2 Electrode Kinetics

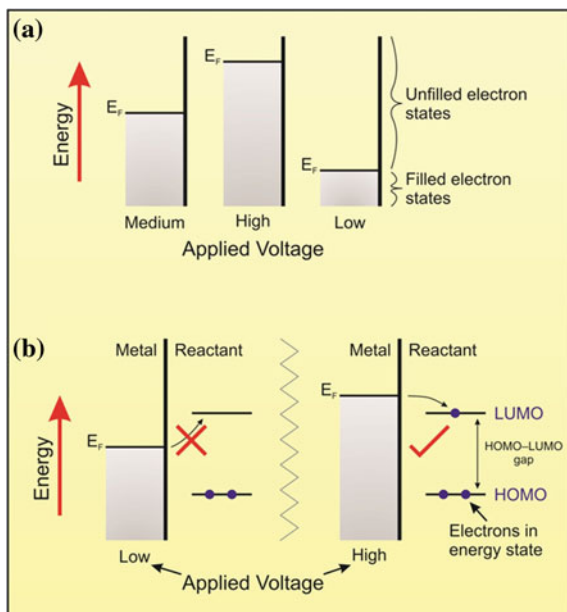
Let us consider the reduction of iron (III) and the oxidation of iron (II):



where the rate constants k_{red} and k_{ox} describe the reduction and oxidation respectively. Note that a cathodic process is one at an electrode (a ‘cathode’) supplying electrons causing a reduction whilst an anodic process is one at an electrode (an ‘anode’) which removes electrons and causes an oxidation process. The rate law for this net process can be described by the following:

$$j = k_{red}[Fe^{3+}]_0 - k_{ox}[Fe^{2+}]_0 \quad (2.11)$$

Fig. 2.5 An overview of ‘driving’ an electrochemical reaction. **a** Band diagram showing the effect of low, medium and high applied voltages. **b** Effect of applied voltage on the Fermi level



where the rate constants k_{red} and k_{ox} are potential dependent with the cathodic reduction dominating at applied negative electrode potentials whilst the anodic oxidation would be the dominant term at applied positive potentials.

Figure 2.6 depicts a reaction profile for the electrochemical process Eq. (2.10) of interest. The dashed line depicts the energy barrier when no potential has been applied, where it can be seen that the process is thermodynamically uphill. When a potential is applied, the free energy of reactants is raised since the Gibbs free energy for the reduction is related to the formal potential by: $\Delta G^0 = -nF(E - E_f^0)$ where $(E - E_f^0)$ measures the potential applied to the working electrode relative to the formal potential of the $\text{Fe}^{3+}/\text{Fe}^{2+}$ couple with *both* potentials measured relative to the same reference electrode. The reaction coordinate changes to that represented by the solid line where it can be seen that the energy required to reach the transition state is lowered and the process is ‘downhill’ and is thus thermodynamically driven.

From inspection of Fig. 2.6, we can write:

$$\Delta G_{red}^{\pm}(2) = \Delta G_{red}^{\pm} + \alpha nF(E - E_f^0) \quad (2.12)$$

and

$$\Delta G_{ox}^{\pm}(2) = \Delta G_{ox}^{\pm} - (1 - \alpha)nF(E - E_f^0) \quad (2.13)$$

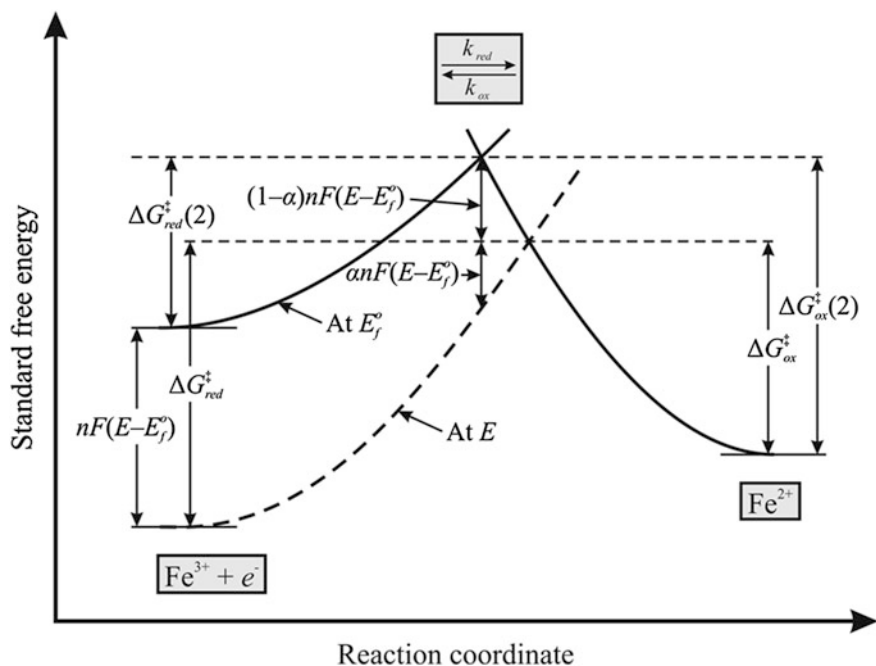


Fig. 2.6 Schematic drawing of the energy profiles along the reaction coordinate for a heterogeneous electron transfer

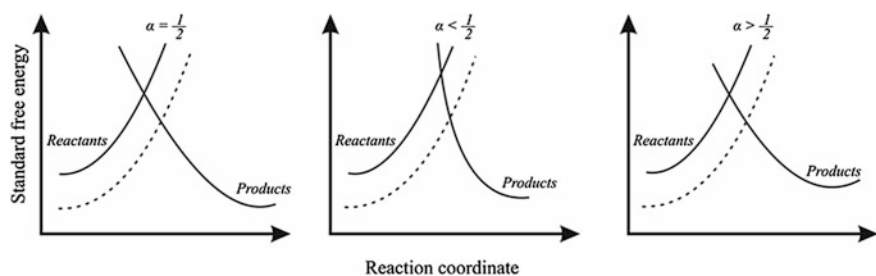


Fig. 2.7 Schematic representation showing the transfer coefficient as an indicator of the symmetry of free energy curve. The dotted line indicates the shift for $\text{Fe}^{3+}(\text{aq}) + e^{-}(m) \xrightleftharpoons[k_{ox}]{k_{red}} \text{Fe}^{2+}(\text{aq})$ as the potential is altered to more positive potentials

where the parameter α is known as the transfer coefficient, which provides physical insights into how the transition state is influenced by the application of voltage and typically is found to have a value of 0.5. A value of one half means that the transition state behaves mid-way between the reactants and products response to applied voltage. Figure 2.7 shows the effect of changing the potential on the free energy curve. In most systems this lies between 0.7 and 0.3 and usually a value of 0.5 is assumed.

Assuming the rate constants, k_{red} and k_{ox} behave in an Arrhenius form:

$$k_{red} = A_{red} \exp(\Delta G_{red}^{\pm}/RT) \quad (2.14)$$

$$k_{ox} = A_{ox} \exp(\Delta G_{ox}^{\pm}/RT) \quad (2.15)$$

Inserting the activation energies (2.12) and (2.13) gives rise to:

$$k_{red} = A_{red} \exp(\Delta G_{red}^{\pm}(2)/RT) \exp(-\alpha nF(E - E_f^0)/RT) \quad (2.16)$$

$$k_{ox} = A_{ox} \exp(\Delta G_{ox}^{\pm}(2)/RT) \exp((1 - \alpha)nF(E - E_f^0)/RT) \quad (2.17)$$

since the first part of Eqs. (2.16) and (2.17) are potential independent we can write:

$$k_{red} = k_{red}^0 \exp(-\alpha nF(E - E_f^0)/RT) \quad (2.18)$$

$$k_{ox} = k_{ox}^0 \exp((1 - \alpha)nF(E - E_f^0)/RT) \quad (2.19)$$

This shows that the electrochemical rate constants for the one electron oxidation of $Fe^{2+}(k_{ox})$ and for the reduction of $Fe^{3+}(k_{red})$ depend exponentially on the electrode potential: k_{ox} increases as the electrode is made more positive relative to the solution whilst k_{red} increases as the electrode is made more negative relative to the solution. It is clear that changing the voltage affects the rate constants. However, the kinetics of the electron transfer is not the sole process which can control the electrochemical reaction; in many circumstances it is the rate of mass transport to the electrode which controls the overall reaction, which we diligently explore later.

We know that the net rate (flux) of reaction is given by: $j = k_{red}[Fe^{3+}]_0 - k_{ox}[Fe^{2+}]_0$. Hence using Eqs. (2.18) and (2.19) we can write:

$$j = k_{red}^0 \exp\left[\frac{-\alpha F(E - E_f^0)}{RT}\right] [Fe^{3+}]_0 - k_{ox}^0 \exp\left[\frac{(1 - \alpha)F(E - E_f^0)}{RT}\right] [Fe^{2+}]_0 \quad (2.20)$$

If we consider the case of a dynamic equilibrium at the working electrode such that the oxidation and reduction currents exactly balance each other then, since no net current flows, $j = 0$ and the fact that $\alpha = 0.5$, we see that:

$$E = E_f^0 + \frac{RT}{F} \ln\left(\frac{[Fe^{2+}]}{[Fe^{3+}]}\right) + \frac{RT}{F} \ln\left(\frac{k_{ox}^0}{k_{red}^0}\right) \quad (2.21)$$

From the discussion earlier it is clear that when no net current flows the potential is given by:

$$E = E_f^0 + \frac{RT}{F} \ln \left(\frac{[Fe^{2+}]}{[Fe^{3+}]} \right) \quad (2.22)$$

so that $k_{ox}^0 = k_{red}^0 = k^0$ which is the *Nernst equation*. Therefore we can write:

$$k_{red} = k^0 \exp \left[\frac{-\alpha F (E - E_f^0)}{RT} \right] \quad (2.23)$$

$$k_{ox} = k^0 \exp \left[\frac{(1 - \alpha) F (E - E_f^0)}{RT} \right] \quad (2.24)$$

Equations (2.23) and (2.24) are the most convenient forms of the *Butler–Volmer expression* for the electrochemical rate constants k_{red}^0 and k_{ox}^0 . The quantity k^0 , with units of cm s^{-1} , is the *standard electrochemical rate constant*

2.3 Mass Transport

Mass transport of the analyte under investigation is governed by the *Nernst-Planck equation* defined by:

$$J_i(x) = -D_i \frac{\partial C_i(x)}{\partial x} - \frac{z_i F}{RT} D_i C_i \frac{\partial \phi(x)}{\partial x} + C_i V(x) \quad (2.25)$$

where $J_i(x)$ is the flux of the electroactive species i ($\text{mol s}^{-1} \text{cm}^{-2}$) at a distance x from the electrode surface, D_i is the diffusion coefficient ($\text{cm}^2 \text{s}^{-1}$), $\frac{\partial C_i(x)}{\partial x}$ is the concentration gradient at distance x , $\frac{\partial \phi(x)}{\partial x}$ is the potential gradient, z_i and C_i are the charge (dimensionless) and concentration (mol cm^{-3}) of species i respectively and $V(x)$ is the velocity (cm s^{-1}) with which a volume element in solution moves along the axis. These three key terms comprising Eq. (2.25) represent the contributions to the flux of species i , that is, diffusion, migration and convection respectively.

If we consider an electrochemical experiment which is conducted in a solution that has supporting electrolyte and in stagnant solutions (non-hydrodynamic conditions, see later) such that migration and convection can be neglected from Eq. (2.25), this is thus reduced to consider the only relevant mode of mass transport to the electrode surface on the experimental time scale, which is diffusion.

The diffusion of species i , from bulk solution to the electrode is described by Fick's first and second laws of diffusion;

$$J_i(x) = -D_i \frac{\partial C_i(x)}{\partial x} \quad (2.26)$$

and

$$\frac{\delta C_i}{\delta t} = -D_i \frac{\partial^2 C_i(x)}{\partial x^2} \quad (2.27)$$

where j is the flux in $\text{mol cm}^2 \text{s}^{-1}$, D the diffusion coefficient in $\text{cm}^2 \text{s}^{-1}$ and C is the concentration of the electro-active species in mol cm^{-3} . In order to obtain the concentrations of the electro-active species at a location x and time t , the partial differential equation should be solved which is possible if the initial (values at $t = 0$) and boundary conditions (values at certain location x) are known.

Let us consider a simple redox process involving the transfer of one-electron between the electrode and species A in solution to form the product B in solution, as shown below;



where the rate of electron transfer is fast compared to the rate of mass transport, *i.e.* an electrochemically and chemically reversible redox process. Assuming that the electron transfer follows Butler–Volmer kinetics,

$$k_{red} = k_{red}^0 \exp\left(\frac{-\alpha F}{RT} \eta\right) \quad (2.29)$$

and

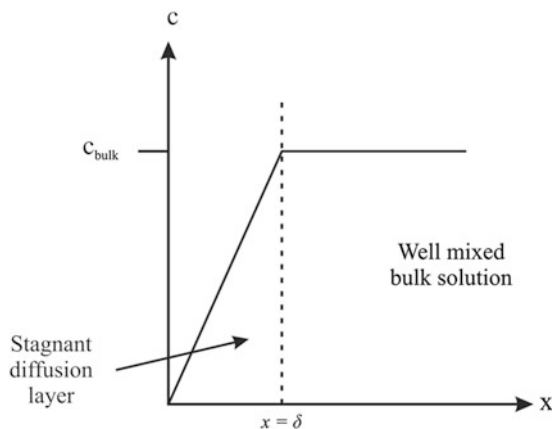
$$k_{ox} = k_{ox}^0 \exp\left(\frac{(1 - \alpha)F}{RT} \eta\right) \quad (2.30)$$

where k^0 is the standard electrochemical rate constant, α is the transfer coefficient of the species under investigation and η is the over-potential defined as:

$$\eta = E - E_{A/B}^{0'} \quad (2.31)$$

where E is the electrode potential and $E_{A/B}^{0'}$ the formal potential for the A/B couple. As electrolysis of A progresses, all of the species A at the electrode surface will be consumed, resulting in a depletion of the concentration of A in the vicinity of the electrode surface and setting up a concentration gradient down which fresh A must diffuse from the bulk solution to support further electrolysis; see Fig. 2.4 which

Fig. 2.8 The Nernst diffusion layer model



depicts the structure of the electrode surface. This depletion zone is known as the diffusion layer, the thickness of which, δ , increases in size as a function of time, t , such that (in one-dimension):

$$\delta = \sqrt{2Dt} \quad (2.32)$$

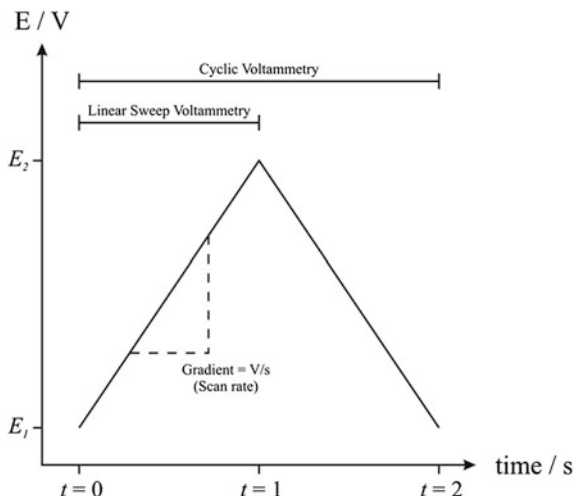
Figure 2.8 depicts the Nernst diffusion layer model which shows that beyond the critical distance, δ , the solution is well mixed such that the concentration of the electroactive species is maintained at a constant bulk value. In this vicinity, the mixing of the solution to even out inhomogeneities is due to ‘natural convection’ induced by density differences. Additionally, if the electrochemical arrangement is not sufficiently thermostated, slight variation throughout the bulk of the solution can provide a driving force for natural convection.

Departing from the bulk solution towards the electrode surface, natural convection dies away due to the rigidity of the electrode surface and frictional forces, this is the diffusion layer, and since only concentration changes occur in this zone, diffusional transport is in operation. Note that in reality there is no real defined zones and these merge into one another, but it is a useful concept. Under experimental conditions, the diffusion layer is in the order of tens to hundreds of micrometers in size.

2.3.1 Cyclic Voltammetry

Cyclic voltammetry is the most extensively used technique for acquiring qualitative information about electrochemical reactions. It tends the rapid identification of *redox* potentials distinctive to the electroactive species under investigation, providing considerable information about the thermodynamics of a redox process, kinetics of heterogeneous electron-transfer reactions and analysis of coupled electrochemical reactions or adsorption processes. Cyclic voltammetry

Fig. 2.9 Potential—time profiles used to perform linear sweep and cyclic voltammetry



consists of scanning (linearly) the potential of the working electrode using a triangular potential wave form (Fig. 2.9).

The potential is swept from E_1 to E_2 and the rate at which this is achieved is the voltammetric scan rate (or the gradient of the line), as shown in Fig. 2.9 (V/s). In this case, if the potential is stopped, this is known as a linear sweep experiment. If the scan is returned back to E_1 , a full potential cycle, this is known as cyclic voltammetry. Depending on the information sought, either single or multiple cycles can be performed. For the duration of the potential sweep, the potentiostat measures the resulting current that arises via the applied voltage (potential). The plot of current *versus* potential (voltage) is termed a ‘cyclic voltammogram’, CV. A cyclic voltammogram is complex and dependent on time along with many other physical and chemical properties.

The *cyclic voltammetric* response can be discovered by solving the transport equations (in three-dimensions, x , y and z) [1]:

$$\frac{\partial[A]}{\partial t} = D_A \nabla^2[A] \quad (2.33)$$

and

$$\frac{\partial[B]}{\partial t} = D_B \nabla^2[B] \quad (2.34)$$

and applying Eqs. (2.29) (2.30) and (2.31) as boundary conditions where the equations [1]:

$$E = E_{start} + vt \quad 0 < t < \frac{E_{end} - E_{start}}{v} \quad (2.35)$$

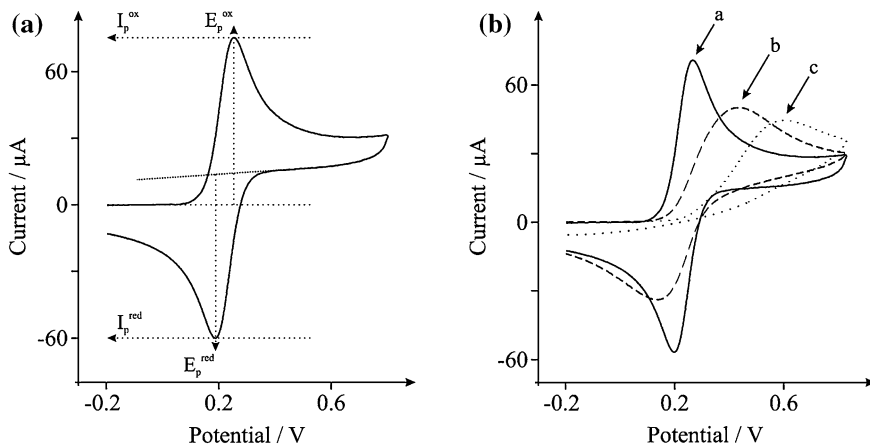


Fig. 2.10 **a** Typical cyclic voltammogram depicting the peak position E_p and peak height I_p . **b** Cyclic voltammograms for reversible (a), quasi-reversible (b) and irreversible (c) electron transfer

and

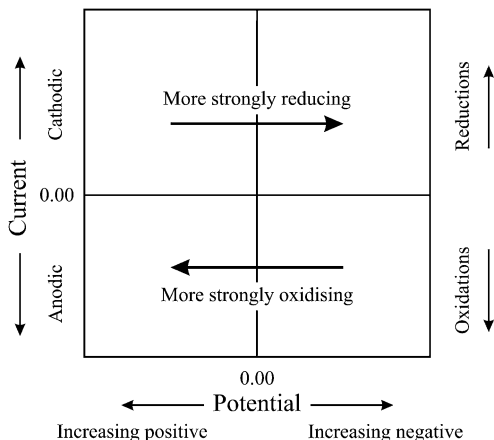
$$E = E_{\text{end}} - v \left[t - \frac{E_{\text{end}} - E_{\text{start}}}{v} \right] \quad (2.36)$$

define the potential sweep between E_{start} and E_{end} with a voltage sweep rate of, v , Vs^{-1} and D_A and D_B are the diffusion coefficients of A and B, respectively.

Figure 2.10 shows a typical cyclic voltammetric curve (or CV) for the case of the electrochemical process as described in Eq. (2.28) where a voltammetric potential is applied and the current monitored which gives rise to the unique profile presented in Fig. 2.10a. Characteristics of the voltammogram which are routinely monitored and reported are the peak height (I_p) and the potential at which the peak occurs (E_p).

It is important to note that in plotting voltammetric data, that is current against potential, there are a number of different axis conventions. In the classical (or *polarographic* using mercury) convention, negative potentials are plotted in the positive “x” direction, thus cathodic currents (due to reductions) are positive; this is shown in Fig. 2.11. In the IUPAC convention, the opposite applies where positive potentials are plotted in the positive “x” direction, thus anodic currents (due to oxidations) are positive (in other conventions, current is plotted along the axis and/or a logarithmic current scale is used). In reality the plotting is dictated by the software that is installed on your potentiostat and your geographic location (for example the USA and related countries favour the classical convention). However, one needs to become familiar with this concept as the literature presents voltammograms in mixed styles and one should ensure on first encountering a

Fig. 2.11 The classical convention for plotting voltammetric data



voltammogram that clarification is sought upon which potential sweep has been applied and understand which currents are anodic and which are cathodic.

Shown in Fig. 2.10b is the case of different heterogeneous electron transfer rates, that is, reversible, quasi-reversible and irreversible, each giving rise to unique voltammetric profiles. The physical processes responsible for the characteristic shape of a ‘reversible’ voltammogram, for the process of $A + ne^- \rightarrow B$, are based on (i) Fick’s laws and (ii) Nernst’s laws:

$$\frac{\partial[A]}{\partial t} = D \frac{\partial^2[A]}{\partial x^2}; \quad \frac{[A]_0}{[B]_0} = e^{\frac{nF\eta}{RT}} \quad (2.37)$$

where the Nernst law is written in the exponential form. It is insightful to consider the diffusion layer at each point in a cyclic voltammetric experiment, which gives rise to the characteristic peak shape observed. Consider the case of electrochemically reversible behaviour. Figure 2.12 shows a typical cyclic voltammogram for $k^0 = 1 \text{ cms}^{-1}$ highlighting concentration—distance plots at six different parts on the voltammetric wave.

In the ‘reversible’ limit the electrode kinetics are so ‘fast’ (relative to the rate of mass transport—see later) that Nernstian equilibrium is attained at the electrode surface throughout the voltammogram with concentrations of A and B at the electrode surface governed by the Nernst equation:

$$E = E_f^0(A/B) + \frac{RT}{F} \ln \frac{[B]_0}{[A]_0} \quad (2.38)$$

where E is now the applied potential which defines the ratio of the surface concentrations $[A]_0$ and $[B]_0$ once $E_f^0(A/B)$ is specified.

Figure 2.12 depicts how the concentration profiles and the surface concentrations change during the voltammogram. Point A on the graph corresponds to the

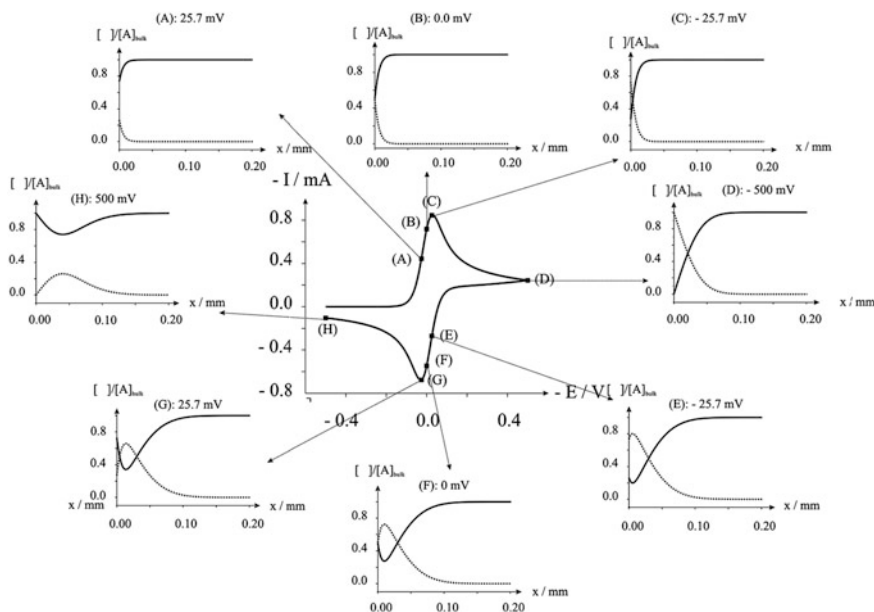


Fig. 2.12 Cyclic voltammogram for the reversible reduction of A to B. Parameters: $E^0 = 0$ V; $\alpha = 0.5$; $k^0 = 1$ cm s⁻¹; $\nu = 1$ Vs⁻¹; $A = 1$ cm²; $[A]_0 = 1$ mM; $D_A = D_B = 10^{-5}$ cm² s⁻¹. The concentration profiles show the distributions of A (solid line) and B (dashed line) at eight location, A–H, on the voltammogram. Reproduced with permission from Ref. [10], with permission from Imperial College Press. Note the negative values of the axis (units) labels

formal potential ($E = E_f^0$). At point A, prior to the start of the peak corresponding to the reduction of A, only a small amount of A has been consumed at the electrode surface and only a small layer of B has consequently built up. This diffusion layer is relatively small, typically in the order of *ca.* 10 μ m. At point C the maximum reduction current in the voltammetric wave is evident and the diffusion layer has increased in thickness. At point D the current is decreasing with increasing potential and the concentration profile plot shows the concentration of A at the electrode surface to be close to zero so that this part of the voltammogram is under diffusion control whereas at (A) it was the electrode kinetics which controlled the response. The diffusion layer at this point has reached a thickness of *ca.* 40 μ m. At point D, the direction of the voltammetric scan is reversed. At point F the working electrode potential has the value of 0 V corresponding to the formal potential of the A/B couple. At this point the electrode potential is insufficient to noticeably reduce A or oxidise B. Point G corresponds to the peak in the reverse scan due to the re-conversion of B to A. The concentration profiles show the build-up of A and depletion of B. Point H corresponds to a point on the reverse peak beyond the maximum G and shows that the concentration of B is very close to zero at the electrode surface whilst that of A has returned to almost its original value nearly that in the bulk solution.

In the case of an electrochemically reversible process *with* fast electron transfer, the peak-to-peak separation $\Delta E_p = (E_p^{ox} - E_p^{red})$ is relatively small at the reversible limit, where $\Delta E_p = 2.218RT/nF$, corresponding to a value of *ca.* 57 mV (at 298 K where $n = 1$). For the case of n electrons, the wave-shape of the voltammogram can be characterised by:

$$E_p - E_{1/2} = 2.218 \frac{RT}{nF} \quad (2.39)$$

where $E_{1/2}$ corresponds to the potential at which half the peak current is observed.

The magnitude of the voltammetric current (I_p^{Rev}) observed at a macroelectrode is governed by the following Randles–Ševčík equation:

$$I_p^{Rev} = \pm 0.446nFAC(nFDv/RT)^{1/2} \quad (2.40)$$

where the \pm sign is used to indicate an oxidation or reductive process respectively though the equation is usually devoid of such sign. The voltammetric diagnosis that the electrochemical process is undergoing a reversible heterogeneous charge transfer process is given by Eq. (2.39) where ΔE_p is independent of the applied voltammetric scan rate and: $I_p^{ox}/I_p^{red} = 1$.

The question is; *how can you determine if your observed voltammetry corresponds to this range?* A key diagnostic is a scan rate study. As shown in Eq. (2.40), the peak height (I_p) is proportional to the applied voltammetric scan rate and a plot of I_p^{Rev} against $v^{1/2}$ should be linear. Figure 2.13 depicts typical voltammetric profiles resulting from applying a range of scan rates. It is evident that each voltammetric signature is the same but that the current increases with increasing scan rate as predicted by Eq. (2.40). It is important to note that when the position of the current maximum occurs at the same potential; this peak maximum, which does *not* shift in potential with scan rate, is characteristic of electrode reactions which exhibit rapid electron transfer kinetics, usually termed reversible electron transfer reactions.

The formal potential can be found as the mid-way between the two voltammetric peaks comprising the voltammogram:

$$E_f^0 = (E_p^{ox} + E_p^{red})/2 \quad (2.41)$$

assuming that the diffusion coefficients of the reactant and product are equal.

Also shown in Fig. 2.10b is the cyclic voltammetric response for an irreversible electrochemical couple (in which the ΔE_p is larger than that observed for the reversible and quasi-reversible case) where appreciable over-potentials are required to drive the reaction, as evidenced by the peak height (maxima) occurring at a greater potential than that seen for the reversible case.

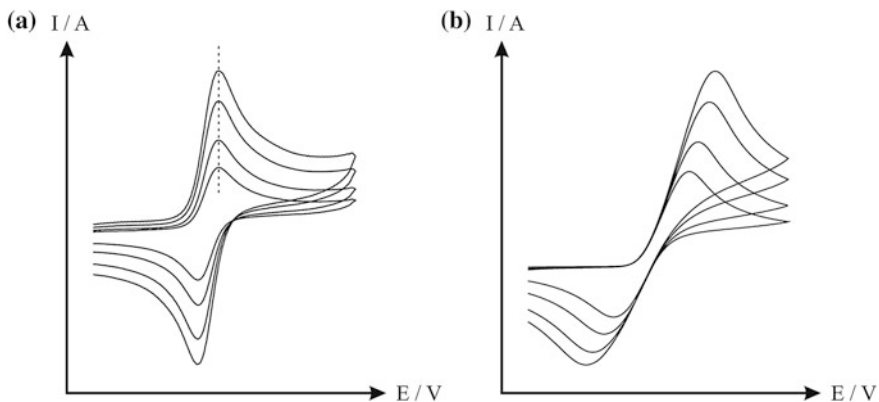


Fig. 2.13 Reversible (a) and irreversible (b) cyclic voltammetric responses. Note the shift of the peak maxima with scan rate

In Fig. 2.10 it is evident that as the standard electrochemical rate constant, k^o , is either fast or slow, termed ‘electrochemically reversible’ or ‘electrochemically irreversible’ respectively, changes in the observed voltammetry are striking. It is important to note that these are relative terms and that they are in relation to the rate of mass transport to the electrode surface. The mass transport coefficient, m_T , is given by:

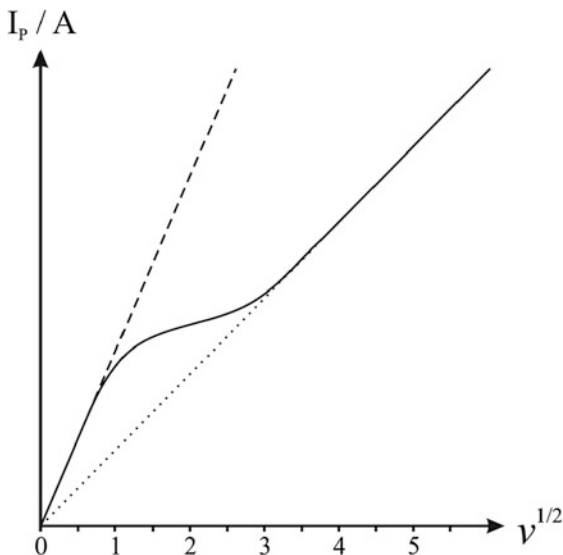
$$m_T = \sqrt{D/(RT/Fv)} \quad (2.42)$$

The distinction between fast and slow electrode kinetics relates to the prevailing rate of mass transport given by ‘ $k^o \gg m_T$ ’ indicating electrochemical reversibility or ‘ $k^o \ll m_T$ ’ indicating electrochemical irreversibility. Matsuda and Ayabe [2] introduce the parameter, ζ , given by:

$$\zeta = k^o/(FDv/RT)^{1/2} \quad (2.43)$$

where the following ranges are identified at a stationary macroelectrode: ‘ $\zeta \geq 15$ ’ corresponds to the reversible limit, ‘ $15 > \zeta > 10^{-3}$ ’ corresponds to the quasi-reversible limit and ‘ $\zeta \leq 10^{-3}$ ’ corresponds to the irreversible limit. Thus returning to Fig. 2.10b, we have three cases, reversible, quasi-reversible and irreversible, which are all related to the rate of mass transport. In reversible reactions the electron transfer rate is, at all potentials, greater than the rate of mass transport and the peak potential is independent of the applied voltammetric scan rate (Fig. 2.13a). In the case of quasi-reversible the rate of electron transfer becomes comparable to the mass transport rate. In this regime, the peak potentials increase with the applied scan rate. Last, it is obvious that for the irreversible case the electron transfer rates are smaller than the rate of mass transport; the summary by Matsuda and Ayabe is extremely useful [2].

Fig. 2.14 Transition from a reversible to an irreversible process with increasing scan rate (*solid line*). The *dashed line* indicates a reversible process, while the *dotted line* is that of an irreversible process



The above conditions given by Matsuda and Ayabe show that the observed electrochemical behaviour depends on the applied voltammetric scan rate. In applying various scan rates the diffusion layer thickness dramatically changes, in the case of slow scan rates, the diffusion layer is very thick while at faster scan rates the diffusion layer is relatively thinner. Since the electrochemical process, that is, reversible or irreversible, reflects the competition between the electrode kinetics and mass transport, faster scan rates will encourage greater electrochemical irreversibility. This is shown in Fig. 2.14 where upon the application of faster scan rates, there is a clear transition (solid line, Fig. 2.14) from that of reversible towards irreversible behaviour.

At macroelectrodes the Nicholson method is routinely used to estimate the observed standard heterogeneous electron transfer rate constant (k^o , cm s^{-1}) for quasi-reversible systems using the following equation [3];

$$\psi = k^o [\pi D n v F / (RT)]^{-1/2} \quad (2.44)$$

where ψ is the kinetic parameter and is tabulated (see Table 2.1) at a set temperature for a one-step, one electron process as a function of the peak-to-peak separation (ΔE_p) where one determines the variation of ΔE_p with v and from this, the variation in the ψ . Table 2.1 shows the variation of ΔE_p with ψ for a one-step, one electron process at 25 °C and where $\alpha = 0.5$. A plot of ψ against $[\pi D n v F / (RT)]^{-1/2}$ allows the standard heterogeneous rate transfer constant, k^o to be readily deduced.

Note that there are some restrictions, in that the above method is based on the assumption that electron transfer kinetics are described by the Butler–Volmer

Table 2.1 Variation of ΔE_p with ψ at 25 °C. Reproduced with permission from Ref. [3]

ψ	$\Delta E_p \times n / \text{mV}$
20	61
7	63
6	64
5	65
4	66
3	68
2	72
1	84
0.75	92
0.50	105
0.35	121
0.25	141
0.10	212

formalism, that α is 0.5, the switching potential is 141 mV past the reversible $E_{1/2}$, and the temperature is 298 K. Lack of strict adherence to most of these factors will lead to only minor errors. However, there is one experimental problem that can be severe: incomplete compensation of solution resistance. As such, measurement error will be low at slow scan rates where currents and IR errors are low, generally however, potentiostats help overcome this problem.

Beyond the limits of the Nicholson method, that is where the ΔE_p is > 200 mV (see Table 2.1), a suitable relationship has been reported by Klingler and Kochi: [4]

$$k^o = 2.18[D\alpha n\nu F/(RT)]^{1/2} \exp\left[-(\alpha^2 nF/RT)(E_p^{ox} - E_p^{red})\right] \quad (2.45)$$

Thus two procedures are available for different ranges of $\Delta E_p \times n$ values, that is for low (Nicholson) and high values (Klingler and Kochi). Lavagnini et al. [5] proposed the following function of ψ (ΔE_p), which fits Nicholson's data, for practical usage (rather than producing a working curve):

$$\psi = (-0.6288 + 0.021X)/(1 - 0.017X) \quad (2.46)$$

where $X = \Delta E_p$. For more accurate results in determining k^o , recourse to electrochemical simulation packages is advised.

The Randles–Ševčík equation for a quasi-reversible system (at 298 K) is given by:

$$I_p^{quasi} = \pm(2.65 \times 10^5)n^{3/2}ACD^{1/2}v^{1/2} \quad (2.47)$$

For an irreversible system (those with slow electron exchange), the individual peaks are reduced in magnitude and widely separated. Figure 2.13 shows a characteristic response where the peak maximum clearly shifts with the applied

voltammetric scan rate. Totally irreversible systems are quantitatively characterised by a shift in the peak potential with scan rate as given by:

$$E_{p,c} = E_f^0 - \frac{RT}{\alpha n' F} \left[0.780 + \ln \frac{D^{1/2}}{k^0} + 0.5 \ln \left(\frac{\alpha n' F v}{RT} \right) \right] \quad (2.48)$$

where α is the transfer coefficient, n' is the number of electrons transferred per mole before the rate determining step and where E_f^0 is the formal potential. Hence, E_p occurs at potentials higher than E_f^0 , with the over-potential related to k^0 and α (the voltammogram becomes increasingly 'drawn out' as αn decreases). For the case of a fully irreversible electron transfer process, the Randles–Ševčík equation is:

$$I_p^{irrev} = \pm 0.496 (\alpha n')^{1/2} n F A C (F D v / RT)^{1/2} \quad (2.49)$$

where A is the geometric area of the electrode (cm^2), α is the transfer coefficient (usually assumed to be close to 0.5), n is the total number of electrons transferred per molecule in the electrochemical process and n' is the number of electrons transferred per mole before the rate determining step. It is useful to know the generic Randles–Ševčík equation (for stagnant solutions):

$$I_p = -\Upsilon(p) \sqrt{\frac{n^3 F^3 v D}{RT}} A [C] \quad (2.50)$$

where : $p = r \sqrt{\frac{n F v}{RT D}}$

for the case of different electrode geometries:

- (1) Planar disc electrode: $r = \text{radius}$, $\Upsilon(p) = 0.446$
- (2) Spherical or hemispherical electrode: $r = \text{radius}$, $\Upsilon(p) = 0.446 + 0.752 p^{-1}$
- (3) For a small disk electrode: $r = \text{radius}$, $\Upsilon(p) = 0.446 + (0.840 + 0.433 e^{-0.66p} - 0.166 e^{-11/p}) p^{-1} \sim 0.446 + 4/\pi p^{-1}$
- (4) For a cylinder or hemi-cylinder: $r = \text{radius}$, $\Upsilon(p) = 0.446 + 0.344 p^{-0.852}$
- (5) For a band electrode: $2r = \text{width}$, $\Upsilon(p) = 0.446 + 0.614(1 + 43.6 p^2)^{-1} + 1.323 p^{0.892} \sim 0.446 + 3.131 p^{-0.892}$

The wave-shape for an irreversible reduction is given by: $E_p - E_{1/2} = 1.857 \frac{RT}{\alpha F}$, while for an irreversible oxidation it is given by: $E_p - E_{1/2} = 1.857 \frac{RT}{(1-\alpha)F}$.

2.4 Changing the Electrode Geometry: Macro to Micro

At a macroelectrode, electrolysis of A occurs across the entire electrode surface such that the diffusion of A to the electrode or B from the electrode surface is termed planar, and the current response is typically described as 'diffusion

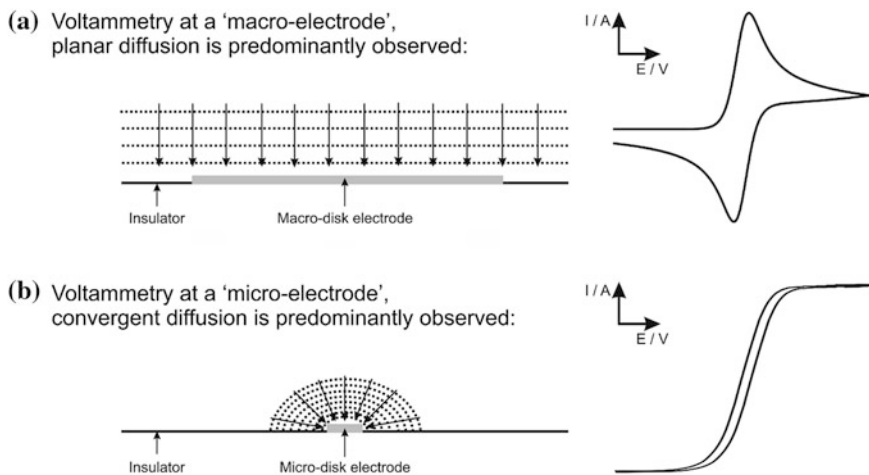


Fig. 2.15 The unique differences between the cyclic voltammetric signatures observed at a macroelectrode (a) compared to a microelectrode (b)

limited', giving rise to an asymmetric peak as shown in Fig. 2.15a. At the edge of the macroelectrode, where the electrode substrate meets the insulating material defining the electrode area, diffusion to or from the edge of the electrode is effectively to a point. Therefore, the flux, j , and the rate of mass transport are larger at the edge and as such diffusion becomes convergent. This is termed an 'edge effect' which is negligible at a macroelectrode since the contribution of convergent diffusion to the edges of the macroelectrode is inundated by that of planar diffusion to the entire electrode area.

As the electrode size is reduced from macro to micro, or even smaller to that of nano, convergent diffusion to the edges of the electrode becomes significant. In this regime a change in the observed voltammetric profile is observed which results in the loss of the peak shaped response, as evident in Fig. 2.15b with that of a sigmoidal voltammogram. The effect of convergent diffusion has the benefit of improvements in mass transport such that the current density is greater than at a macroelectrode under planar diffusion.

For a reversible electrode reaction at a microelectrode, as shown in Fig. 2.15b, where $E_{1/2}$ is the half-wave potential, the following equation describes the expected voltammetric shape:

$$E = E_{1/2}^{rev} + \frac{RT}{nF} \ln \frac{I_L - I}{I_L}$$

$$\text{where } E_{1/2}^{rev} = E^{0'} + \frac{RT}{nF} \ln \frac{D_R^{1/2}}{D_O^{1/2}} \quad (2.51)$$

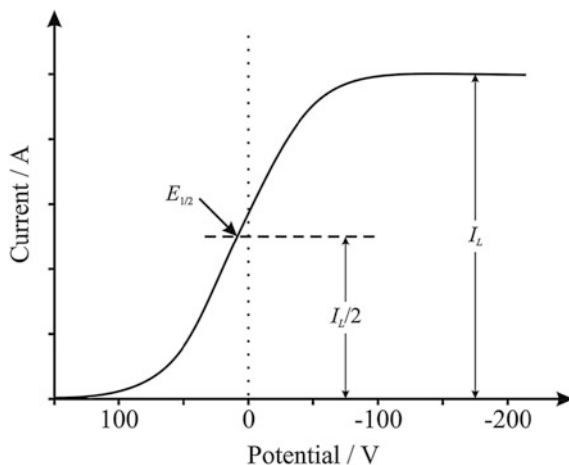


Fig. 2.16 Steady state voltammogram for a reversible process observed at a microelectrode

since the ratio of diffusion coefficient is nearly equal, $E_{1/2}$ is a good approximation for $E^{0'}$ for a reversible couple (Fig. 2.16).

When a plot of E against $\ln \frac{I_L - I}{I_L}$ is constructed, a linear response should be observed with a gradient equal to RT/nF and an intercept of $E_{1/2}^{rev}$ if the wave-shape corresponds to a reversible process. The effect of different electrochemical kinetics is shown for the case of a microelectrode in Fig. 2.17, where the voltammogram is shifted as the electron transfer becomes slower since a greater ‘overpotential’ is needed to overcome the kinetic barrier. In this case, Eq. (2.51) becomes: $E = E_{1/2}^{irr} + \frac{RT}{nF} \ln \frac{I_L - I}{I_L}$. Thus a plot of E against $\ln \frac{I_L - I}{I_L}$ gives rise to a gradient of $\frac{RT}{nF}$ and an intercept of $E_{1/2}^{irr}$.

To determine between reversible, quasi-reversible and irreversible, a useful approach is the Tomeš criteria; [7] see Ref. [6] for a full overview of the various diagnostic approaches.

Last, Fig. 2.18 shows the different microelectrode geometries that can be readily encountered in electrochemistry. For an elegant overview of microelectrodes and their benefits and applications, readers are directed to Ref. [7].

2.5 Electrochemical Mechanisms

Above we have considered an E reaction where the (electrochemical) process involves the transfer of an electron. If we now consider that this process is perturbed by a subsequent chemical reaction, as described by:



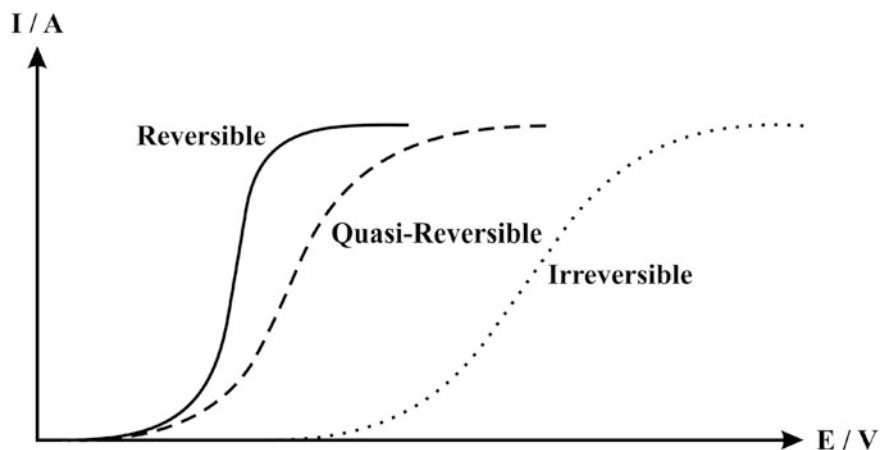


Fig. 2.17 How a steady-state voltammogram is shaped by electrochemical (heterogeneous) kinetics

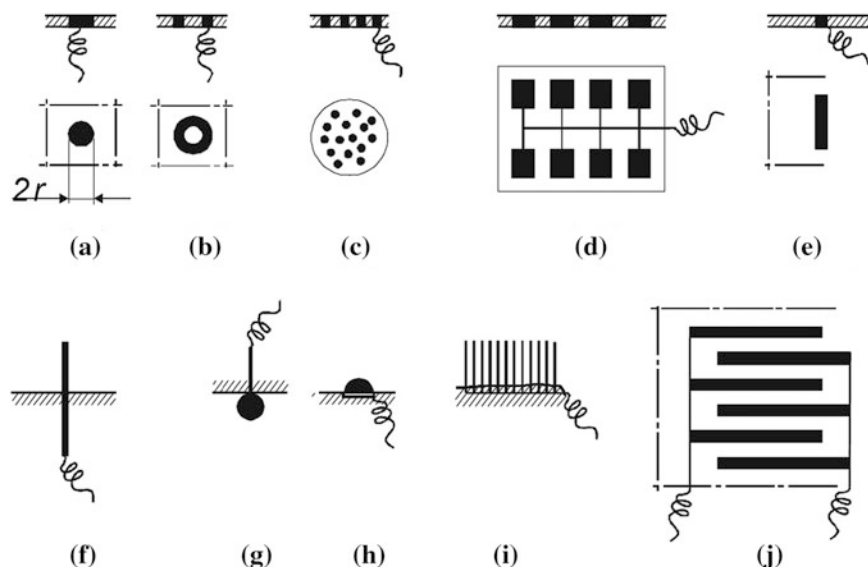
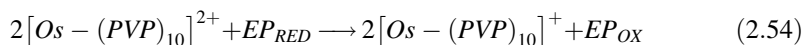
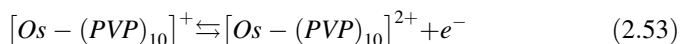


Fig. 2.18 The most important geometries of microelectrodes and microelectrode arrays; **a** microdisk; **b** microring; **c** microdisk array (a composite electrode); **d** lithographically produced microband array; **e** microband; **f** single fibre (microcylinder); **g** microsphere; **h** microhemisphere; **i** fibre array; **j** interdigitated array. Image reproduced with permission from Ref. [7], copyright 2000 International Union of Pure and Applied Chemistry

using the notation of Testa and Reinmuth [8] this is described as an *EC* reaction. The cyclic voltammogram will display a smaller reverse peak (because the product *R* is chemically removed from the surface). The peak ratio of the forward and reverse peaks will thus be less than 1 (not equal); the exact value can be used to estimate the rate constant of the chemical step. In some (extreme) cases, the chemical reaction may progress so rapidly that all of *R* is converted to *Z*, resulting in no reverse wave being observed. Note that by varying the scan rate, further information on the rates of these coupled reactions can be obtained. Table 2.2 overviews the different electrochemical mechanisms involving coupled chemical reactions that can be encountered.

A specific example worth exploring is the *EC'* reaction. Such an example of this process is the modification of a glassy carbon electrode with an Osmium polymer, $[\text{Os}(\text{bpy})_2(\text{PVP})_{10}\text{Cl}]\text{Cl}$ and Nafion prepared by drop-coating, producing a double-layer membrane modified electrode [9]. In this case the modified electrode was explored towards the sensing of the neurotransmitter epinephrine (EP) [9]. Figure 2.19 shows the voltammetric response of the electroactive polymer (curves A and B in Fig. 2.19) where upon contact with epinephrine (curve C in Fig. 2.19) a reduction in the back peak coupled with an increase in the forward wave is evident. The process can be described as:



The first step in the above Eqs. (2.53) and (2.54) is the *E* step due to it being a purely electrochemical process, while the process in Eq. (2.54) is noted as a *C* step due to it being a chemical process. As shown in Fig. 2.19, the magnitude of curve C is dependent upon the chemical rate constant for the process as governed by Eq. (2.54).

Another electrochemical process worth highlighting, which demonstrates how cyclic voltammetry can be used to yield mechanistic information, is an *EE* process. Here we take the example of TMPD (N,N,N',N'-tetramethylphenylenediamine), the structure of which is shown in Fig. 2.20. Figure 2.21 shows the cyclic voltammogram recorded for the oxidation of TMPD in an aqueous solution (pH 7 phosphate buffer solution, PBS) utilising an EPPG electrode. The two voltammetric peaks, as shown in Fig. 2.21a, represent the following electrochemical process:

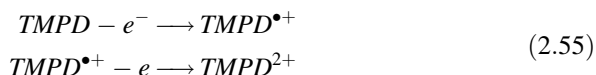
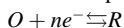
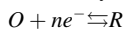
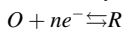
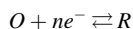
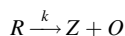
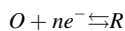
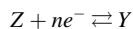
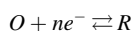
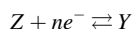
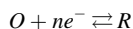
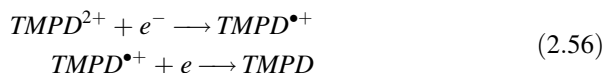


Table 2.2 Electrochemical mechanisms involving coupled chemical reactions

 Reversible electron transfer process, no follow-up chemistry; an E_r step:

 Reversible electron transfer process followed by a reversible chemical reaction; E_rC_r :

 Reversible electron transfer process followed by an irreversible chemical reaction; E_rC_i :

 Reversible chemical reaction preceding a reversible electron transfer process; C_rE_r :

 Reversible electron transfer processes followed by an irreversible regeneration of starting materials; E_rC_i'

 Multiple electron transfer processes with an intervening reversible chemical reaction; $E_rC_rE_r$:

 Multiple electron transfer processes with an intervening irreversible chemical reaction; $E_rC_iE_r$:


where the cation radical and the dication are shown in Fig. 2.22. On the reverse scan, the corresponding reduction takes place;



The voltammetric response, as shown in Fig. 2.21b is recorded at a slower scan rate than that used in Fig. 2.21a and it is evident that the second reduction peak, corresponding to the reduction of TMPD^{2+} , has significantly changed. This is because in the case of Fig. 2.21b the time taken to scan the voltammetric window is long in comparison with the lifetime of the electro-generated species (formed on the forward scan). In fact, TMPD^{2+} reacts with water with the displacement of

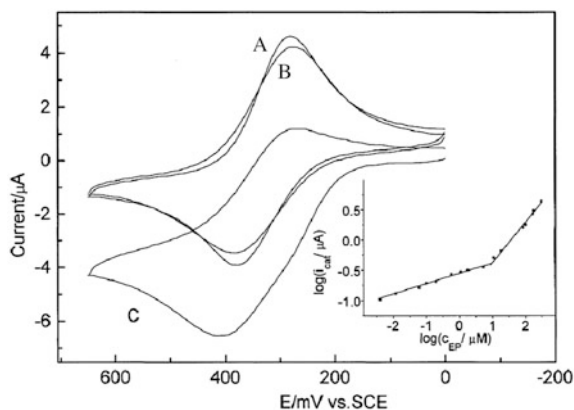


Fig. 2.19 Cyclic voltammograms of Os-(PVP)₁₀ (A) and Os-(PVP)₁₀/Nafion (B, C) modified electrodes in pH 6.9 PBS (A, B) and (B), + 1.0×10^{-4} M epinephrine (C) at a scan rate of 40 mV s^{-1} . Inset: plot of logarithm of catalytic current versus epinephrine concentration. Figure reproduced from Ref. [9] with permission from Elsevier

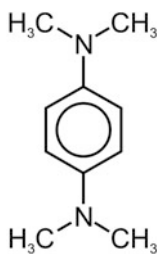


Fig. 2.20 The structure of TMPD

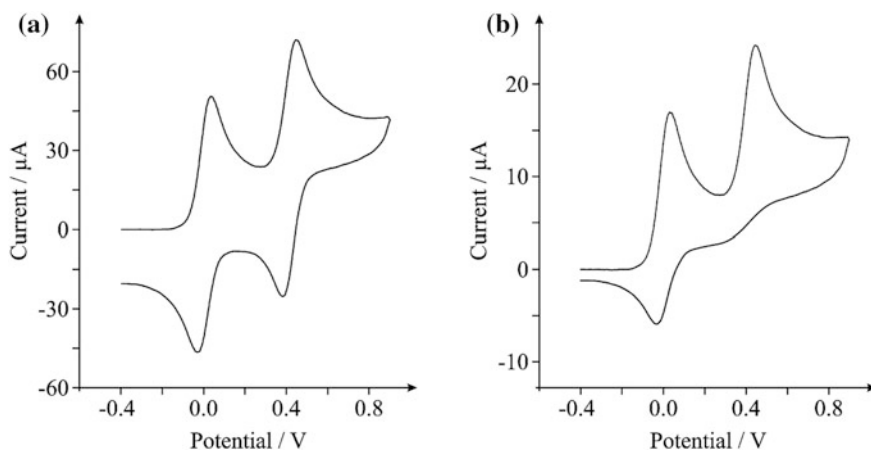


Fig. 2.21 Cyclic voltammograms obtained from the electrochemical oxidation of TMPD at a scan rate of **a** 100 mVs^{-1} and **b** 10 mVs^{-1}

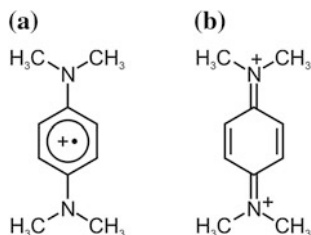


Fig. 2.22 The structures of **a** the cation radical TMPD^{1+} and **b** the dication TMPD^{2+}

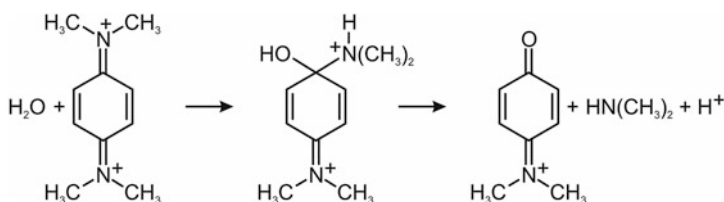


Fig. 2.23 TMPD^{2+} reacts with water with the displacement of dimethylamine

dimethylamine, as shown in Fig. 2.23 and hence on the timescale of the voltammetric experiment the electro-generated species undergoes a chemical reaction such that the initially formed product cannot be electrochemically reduced on the return voltammetric scan. Note that this is not the case when using fast scan rates where the time taken to scan the voltammetric window is fast in comparison to the lifetime of the electro-generated species such that the chemical process is outrun.

Hence, given the above insights, it is clear that cyclic voltammetry can be used to provide a facile methodology to study unstable and exotic species.

2.6 Effect of pH

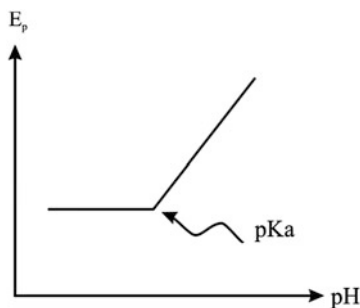
Consider the following process involving the uptake of m -protons and consumption of n -electrons:



The limiting cases correspond to those of electrochemical reversibility and irreversibility. Here we consider the electrode process being fully electrochemically reversible, thus for the relevant Nernst equation we can write [10]:

$$E = E_f^0(A/B) - \frac{RT}{nF} \ln \frac{[B]}{[A][\text{H}^+]^m} \quad (2.58)$$

Fig. 2.24 A typical plot of peak potential, E_p versus pH



$$E = E_f^0(A/B) + \frac{RT}{nF} \ln[H^+]^m - \frac{RT}{nF} \ln \frac{[B]}{[A]} \quad (2.59)$$

$$E = E_f^0(A/B) - 2.303 \frac{mRT}{nF} pH - \frac{RT}{nF} \ln \frac{[B]}{[A]} \quad (2.60)$$

leading to:

$$E_{f, eff}^0 = E_f^0(A/B) - 2.303 \frac{mRT}{nF} pH \quad (2.61)$$

where $E_{f, eff}^0$ is an effective formal potential. Provided $D_A = D_B$ the potential midway between the peaks for the reduction of A and the oxidation of B corresponds to $E_{f, eff}^0$ with the shape of the voltammogram being otherwise unaffected. Accordingly the midpoint potential varies by an amount of $2.303 \frac{mRT}{nF}$ per pH unit. In the commonly seen case where $m = n$, this corresponds to *ca.* 59 mV per pH unit at 25 °C as in the following case.

Experimentally, the cyclic voltammetric response is recorded over a range of pH's with the $E_{f, eff}^0$ (or more commonly 'peak potential') plotted as a function of pH. Figure 2.24 shows a typical response where the deviation from linearity is due to the pK_a of the target analyte and the gradient from the linear part allows information on the number of electrons and protons transferred in the electrochemical process.

A real example from the literature is shown in Fig. 2.25 which utilises a catechin-immobilised poly(3,4-ethylenedioxythiophene)-modified electrode towards the electrocatalysis of NADH in the presence of ascorbic acid and uric acid [11]. Interestingly, catechin has a quinone moiety in its oxidised state and the effect of pH on the redox properties of the modified electrode is shown in Fig. 2.25 over the pH range of 2–10 where the redox couple of the catechin molecules are shifted to less positive values with the increase in pH. The insert in Fig. 2.25 shows a plot of the half-wave potential of the catechin molecule as a function of pH. Note it

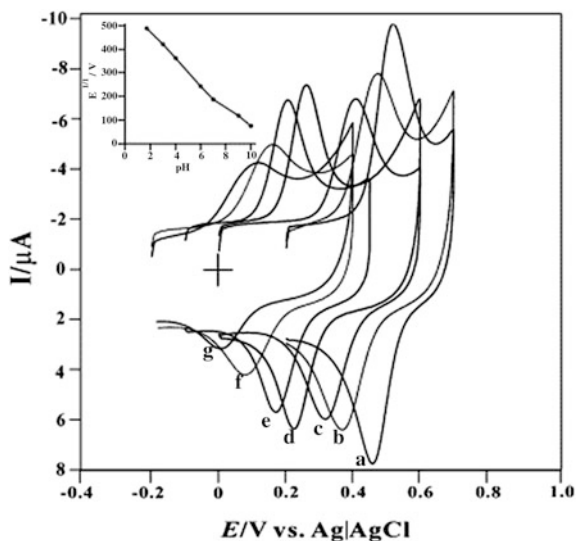
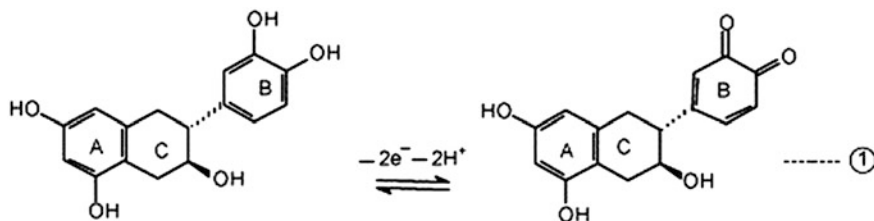
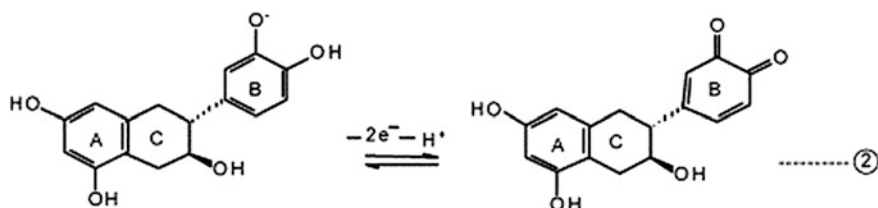


Fig. 2.25 Example from the literature: cyclic voltammograms of the catechin/PEDOT/GC-modified electrode in PBSs of various pH: **a** 1.5; **b** 3; **c** 4; **d** 6; **e** 7; **f** 9 and **g** 10. Inset: plot of $E_{1/2}$ versus pH. Reproduced from Ref. [11] with permission from Elsevier



Scheme 2.1 Electrochemical mechanism of an equal electron and proton transfer process at the catechin molecule. Reproduced from Ref. [11] with permission from Elsevier

resemblance to that of Fig. 2.24. It is evident that there are two slopes, the first corresponds to 63 mV/pH over the pH range of 1–7.5 which is very close to the anticipated Nernstian value for the same number of electron and proton transfer processes (Scheme 2.1). In the above example, it is expected that this corresponds to two electrons and two protons involved during the oxidation of catechin to its *o*-quinone form. The second slope is evident in the pH range of 7.5–10; a slope of 33 mV/pH is obtained which is very close to the Nernstian value for a two-electron and one-proton process (Scheme 2.2). Additionally, the authors [11] report a gradual decreases in the peak currents in this pH range which they attribute to the deprotonation of catechin molecules, which leads to an increase in the charge on the catechin molecules where the charged species is more soluble than the former



Scheme 2.2 Electrochemical mechanism of a two-electron and one-proton transfer process at the catechin molecule. Reproduced from Ref. [11] with permission from Elsevier

species. Clearly the use of pH measurements can help provide insights into electrochemical mechanisms.

2.7 Other Voltammetric Techniques: Chronoamperometry

In the above part of the *Handbook*, we have considered cyclic voltammetry and its derivatives. Another technique that is worthy of mention, and that can be used to study graphene, is chronoamperometry. This technique is commonly used either as a *single potential step*, in which only the current resulting from the forward step (as described above) is recorded, or *double potential step*, in which the potential is returned to a final value following a time period, usually designated as τ , at the step potential. The electrochemical technique of chronoamperometry involves stepping the potential applied to the working electrode, where initially it is held at a value at which no Faradaic reactions occur before jumping to a potential at which the surface concentration of the electroactive species is zero (Fig. 2.26a), where the resulting current-time dependence is recorded (Fig. 2.26c).

The mass transport process throughout this process is solely governed by diffusion, and as such the current-time curve reflects the change in concentration at the electrodes surface. This involves the continuing growth of the diffusion layer associated with the depletion of reactant, thus a decrease in the concentration gradient is observed as time progresses (Fig. 2.26b). An example of single potential step chronoamperometry is shown in Fig. 2.27 for the case of an Osmium complex modified electrode and also shown in the inserts are the effect of concentration of epinephrine which is electro-catalysed undergoing an EC' process (see Sect. 2.5).

The most useful equation in chronoamperometry is the Cottrell equation, which describes the observed current (planar electrode of infinite size) at any time following a large forward potential step in a reversible redox reaction (or to large overpotential) as a function of $t^{-1/2}$.

$$I_L(t) = nFAD^{1/2}C(\pi t)^{-1/2} \quad (2.62)$$

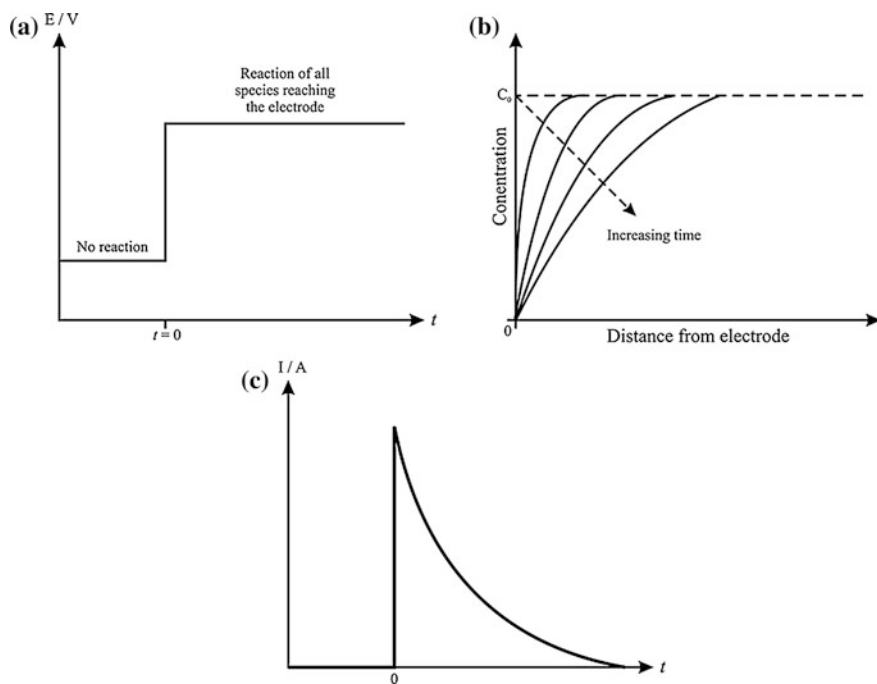


Fig. 2.26 Chronoamperometric experiment: **a** potential-time waveform; **b** change of concentration gradient; **c** resulting current-time response

where n = stoichiometric number of electrons involved in the reaction, F is the Faraday's constant, A is the electrode area, C is the concentration of electroactive species and D is the diffusion coefficient. The current due to double layer charging also contributes following a potential step but decays as a function of $1/t$ and is only significant during the initial period, typically a few milliseconds following the potential step.

A variant on the chronoamperometry as discussed in Fig. 2.27 is that presented in Fig. 2.28, which is where a hybrid biointerface electrode, consisting of a gold nanoparticle (AuNP) and *cytochrome c* (cyt *c*) on indium tin oxide (ITO) platform, is explored towards the sensing of hydrogen peroxide. In this example, the potential is held at a value, which induces the desired electrochemical reaction, and the solution is stirred such that a convective flow is induced. Aliquots of the analyte under investigation are made and at each time, the convective flow ensures that the species is transported to the electrode surface and is electrochemically transformed; this is recognised in Fig. 2.28 by a 'step' in the current which then plateaus or reduces as all the electroactive species are consumed. Analysis of the 'steps', as evident in Fig. 2.28, yields the corresponding calibration plot. Such an approach, where convection is used to enhance the rate of mass transport to the electrode surface, is known as hydrodynamic electrochemistry and offers

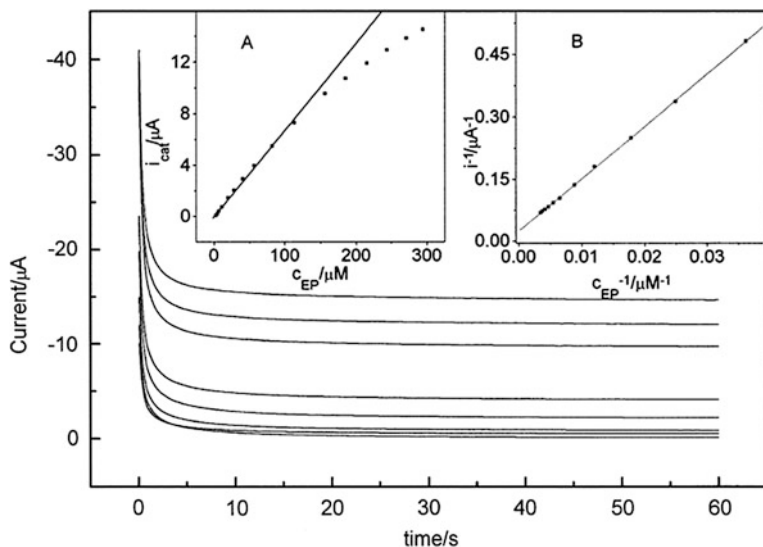


Fig. 2.27 Example from the literature: chronoamperometric curves with a potential step from 0 to +0.4 V at Os-(PVP)₁₀/Nafion modified electrode in pH 6.9 PBS containing 0, 6.5, 11, 28, 56, 156, 215 and 294 μM (from *bottom to top*). Inset: *A* plot of catalytic current versus epinephrine concentration; *B* data analysis of catalytic current versus epinephrine concentration. Reproduced from Ref. [9] with permission from Elsevier

improvements in the analytical sensitivity in comparison to measurements performed in stagnant solution (Fig. 2.27).

Double potential step chronoamperometry is illustrated in Fig. 2.29 for the electrochemical oxidation of ferrocene (Fc) to ferrocenium (Fc⁺). Double potential step chronoamperometry is extremely useful as it allows simultaneous determination of the diffusion coefficients of the initial species, in this example, ferrocene, and of the product of the electrochemical reaction, ferrocenium. Figure 2.29 shows typical chronoamperometry currents recorded at different temperatures using a microelectrode where the sample was pre-treated by holding the potential at a point corresponding to zero Faradaic current for 20 s, after which the potential was stepped to a position after the peak (as determined via CV) and the current measured for 5 s. The potential was then stepped back to the initial value and the current measured for a further 5 s. Note that for chronoamperometry at a microelectrode, Eq. (2.62) is replaced by:

$$I_L(t) = nFADC \left[(\pi Dt)^{-1/2} + r^{-1} \right] \quad (2.63)$$

which turns back into Eq. (2.62) if $r \rightarrow \infty$.

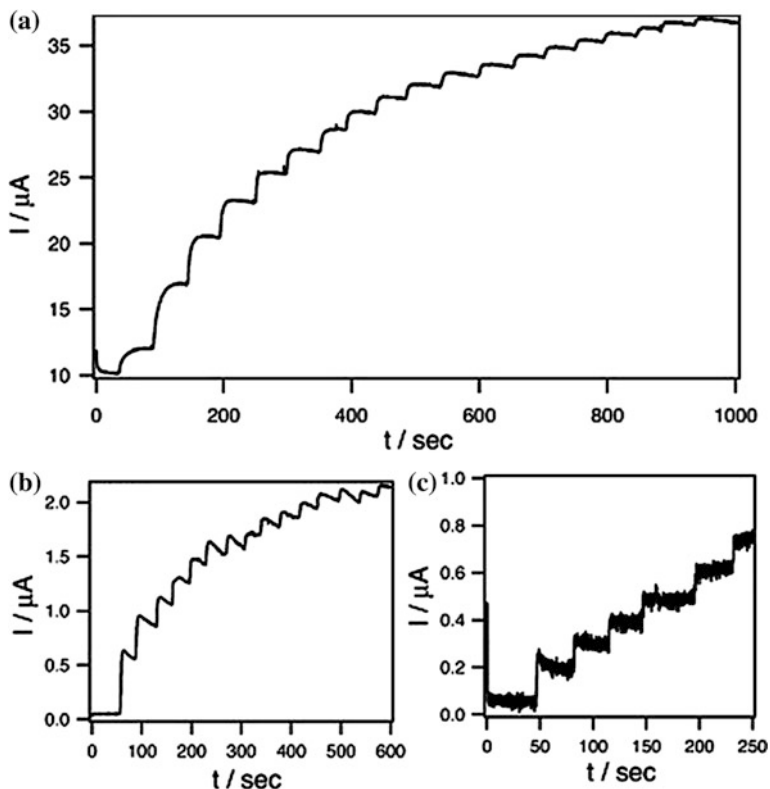


Fig. 2.28 Example from the literature: current–time curve obtained for **a** ITO/AuNP/*cyt c* electrode upon successive addition of 20 μL aliquots of 200 mM H_2O_2 to 5 mL stirred 10 mM HEPES buffer at pH 7 with an applied potential of -0.1 V under nitrogen atmosphere; chronoamperometric curve obtained for **b***cyt c*/ITO and **c** AuNP/ITO obtained by the addition of 20 μL aliquots of 200 mM H_2O_2 in 5 mL stirred solution of 10 mM HEPES buffer at the potential of -0.1 V under nitrogen atmosphere. Reproduced from Ref. [29] with permission from Elsevier

The time-dependent current response obtained on the first step (see Fig. 2.29) was analysed via the use of the following equation, as proposed by Shoup and Szabo [12], which sufficiently describes the current response over the entire time domain, with a maximum error of less than 0.6 %:

$$I = -4nFDrCf(\tau) \quad (2.64)$$

where

$$f(\tau) = 0.7854 + 0.8863\tau^{-1/2} + 0.2146\exp(-0.7823\tau^{-1/2}) \quad (2.65)$$

and where the dimensionless time parameter, τ is given by:

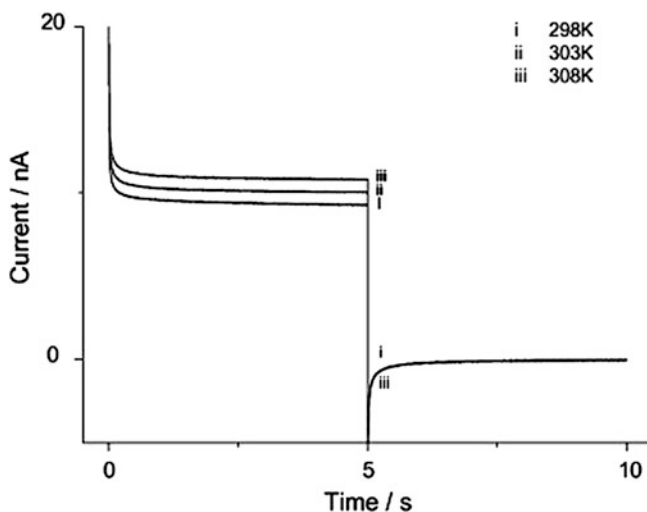


Fig. 2.29 Experimental double potential step chronoamperometric transients for the $\text{Fc}|\text{Fc}^+$ system at temperatures of *i* 298 *ii* 303 and *iii* 308 K. The potential was stepped from 0.0 to 0.9 and back to 0.0 V. Reproduced from Ref. [30] with permission from Elsevier

$$\tau = 4Dt/r^2 \quad (2.66)$$

Theoretical transients were generated using the above equation and a nonlinear curve fitting function available in certain software (such as OriginPro 7.5—Microcal Software Inc.). The fit between the experimentally observed response and theoretical data was optimised by inputting a value for r , which is independently characterised using model solutions and instructing the software to iterate through various D and nc values. Figure 2.30 shows a typical fit of experimental and simulated results using Eqs. (2.64), (2.65) and (2.66).

2.7.1 Experimental Determination of Diffusion Coefficients

The double potential step method is often applied in the measurement of rate constants for chemical reactions (including product adsorption) occurring following the forward potential step. Chronoamperometry can also be used to determine an accurate measurement of electrode area (A) by use of a well-defined redox couple (known n , C , and D). Other uses are in extracting nucleation rates (see for example: [13–17]) and uses in sensing, as shown in Figs. 2.27 and 2.28, to name just a few. In some instances, when one is experimentally measuring a diffusion coefficient of a target analyte which has not been reported before, one needs to know that the

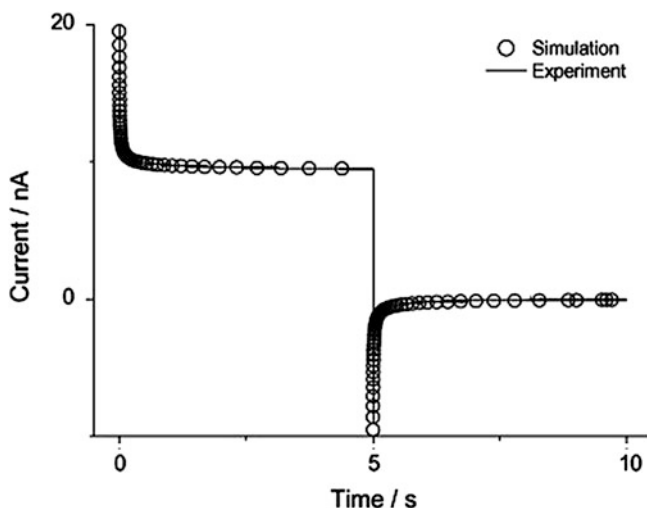


Fig. 2.30 Experimental (—) and best-fit theoretical (○) double potential step chronoamperometric transients for the $\text{Fc}|\text{Fc}^+$ system at a temperature of 298 K in MeCN with 0.1 M TBAPF₆ supporting electrolyte. The potential was stepped from 0.0 to 0.9 and back to 0.0 V. Reproduced from Ref. [30] with permission from Elsevier

correct number (or order of magnitude) has been derived. To this end, a model for estimating the diffusion coefficients has been proposed by Wilke and Chang: [18]

$$D = 7.4 \times 10^{-8} \frac{(xM)^{1/2} T}{\eta V^{0.6}} \quad (2.67)$$

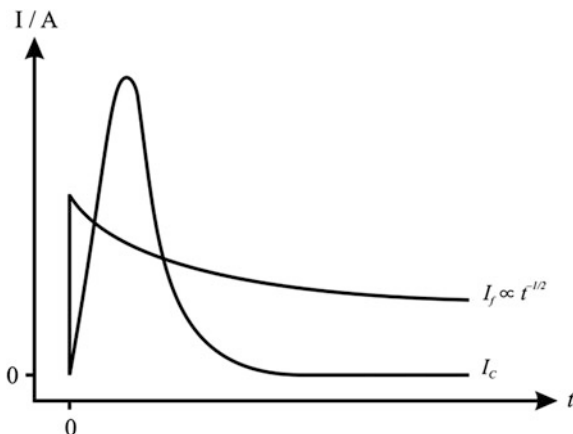
where M is the relative molar mass of the solvent, η is its viscosity, x is an association parameter and V is the molar volume of the solute, estimated for complex molecules by summation of atomic contributions [18].

2.8 Other Voltammetric Techniques: Differential Pulse Voltammetry

As introduced earlier, voltammetry so far has been concerned with applying a potential step where the response is a pulse of current which decays with time as the electroactive species near the vicinity of the electrode surface are consumed. This Faradaic process (I_F) is superimposed with a capacitive contribution (I_C) due to double layer charging which dies away much more quickly, typically within microseconds (see Fig. 2.31).

The current (for a reversible system) is in the form of the Cottrell Equation where $I \propto t^{-1/2}$ and charge, Q , is $Q \propto t^{1/2}$. When a step in pulse is applied the

Fig. 2.31 Effect of capacitive and Faradaic current following the application of a potential step



current is sampled when the capacitive current (I_c) decays away. To achieve this pulse widths are chosen to meet this condition.

In pulse techniques such as differential pulse and square wave voltammetry, the capacitive contribution is eliminated via subtraction. Differential pulse voltammetry (DPV) measures the difference between two currents just before the end of the pulse and just before its application. Figure 2.32 shows the waveform of pulse utilised which is superimposed on a staircase.

The base potential is implemented in a staircase and the pulse is a factor of 10 or more shorter than the pulse of the staircase waveform. The difference between the two sampled currents is plotted against the staircase potential leading to a peak shaped waveform as shown in Fig. 2.33.

For a reversible system the peak occurs at a potential: $E_p = E_{1/2} - \Delta E/2$ where ΔE is the pulse amplitude. The current is given by:

$$I_p = \frac{nFAD^{1/2}C}{\pi^{1/2}t^{1/2}} \left(\frac{1 - \alpha}{1 + \alpha} \right) \quad (2.68)$$

where

$$\alpha = \exp(nF\Delta E/2RT) \quad (2.69)$$

DPV is useful due to eliminations in the contribution of non-faradaic (capacitive) processes, which are effectively subtracted out. The power of DPV is evident from inspection of Fig. 2.34 for the supercoiled plasmid DNA where poor electrochemical signals obtained using linear sweep voltammetry are transformed into quantifiable and beautiful voltammetric signatures.

Additionally, DPV is useful for resolving the voltammetric signals due to two species with close half-wave potentials, producing easily quantifiable peak shaped responses. This is exemplified in Fig. 2.35 for the simultaneous sensing of ascorbic

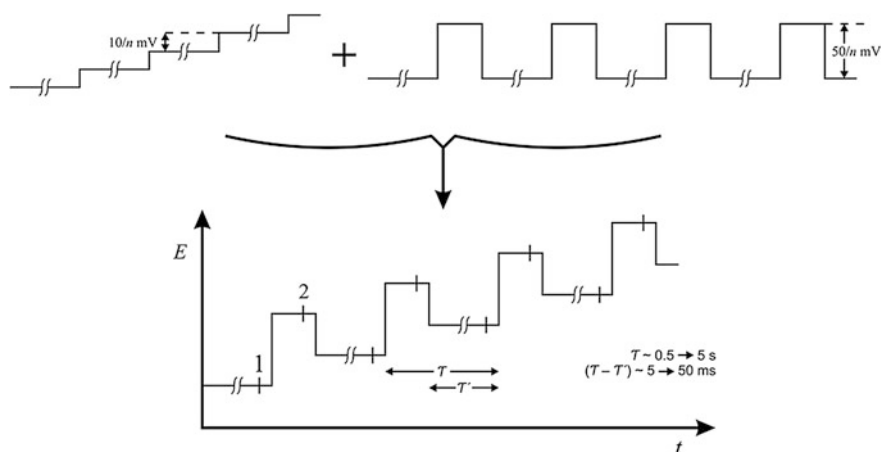


Fig. 2.32 Differential pulse voltammetry waveform of pulses superimposed on a staircase

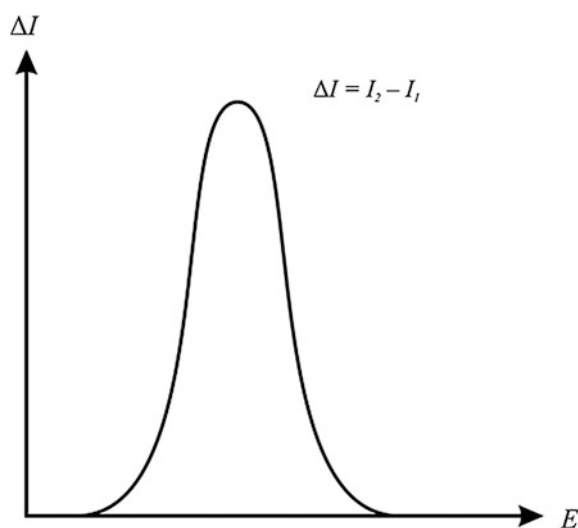


Fig. 2.33 Differential pulse voltammetry; voltammetric profiles of ΔI versus staircase potential

acid and acetaminophen which are well known to cause problems due to their overlapping voltammetric responses.

Figure 2.35 compares CV and DPV using a range of modified electrodes. In all cases, two sharp and well-resolved peaks are observed when DPV is utilised; in this analytical case, the resulted separation in the two peak potentials is sufficient enough to achieve the accurate simultaneous determination of ascorbic acid and acetaminophen in real samples [19].

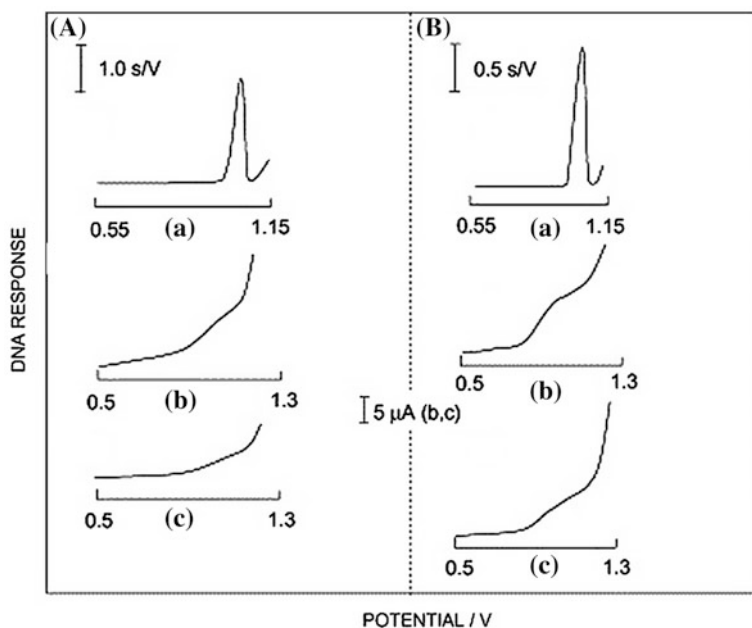


Fig. 2.34 Differential pulse (a) and linear scan (b, c) voltammograms for $15 \mu\text{g mL}^{-1}$ supercoiled plasmid DNA (A) and $15 \mu\text{g mL}^{-1}$ linearised DNA (B) at carbon paste electrodes. The anodic signal corresponds to the electrochemical oxidation of DNA-G residues. Reproduced from Ref. [31] with permission of Elsevier

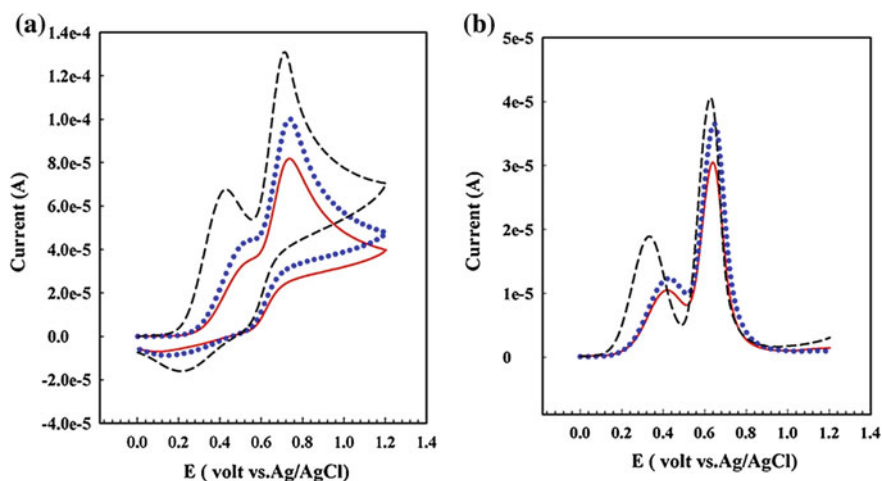


Fig. 2.35 a Cyclic and b differential pulse voltammograms of 0.1 mM ascorbic acid and 0.1 mM acetaminophen in acetate buffer solution (0.1 M, pH 4.0) on the surface of various electrodes; unmodified carbon paste electrode (solid line), CNT-carbon paste electrode (dotted line) and multi-walled carbon nanotube/thionine modified electrode (dashed line). Sweep rate was 100 mV s^{-1} . Reproduced from Ref. [19] with permission of Elsevier

Note that such a response is obtained through increasing the pulse amplitude (see Fig. 2.32) but in doing so, the peak width also increases, meaning that, in practice, ΔE values of more than 100 mV are not viable; careful optimisation of the electrochemical parameters is clearly required. The expression for the half-width at half-height, $W_{1/2}$; where $W_{1/2} = 3.52RT/nF$ leads to a value of 90.4 mV for $n = 1$ at 298 K showing that peaks separated by 50 mV may often be resolved. Detection limits of DPV can be realised at *ca.* 10^{-7} M.

Recently it has been highlighted that the literature is not consistent and that actually the waveform presented in Fig. 2.32, should be termed “Differential Multi Pulse Voltammetry” [20]. Figure 2.36 shows the range of waveforms that can exist.

Differential Double Pulse Voltammetry (DDPV), where the length of the second pulse (t_2) is much shorter than the length of the first pulse (t_1), $t_1/t_2 = 50\text{--}100$ (Fig. 2.36a), which leads to very high sensitivity. *Differential Double Normal Pulse Voltammetry (DDNPV)* is where both pulses have similar durations $t_1 \approx t_2$ (Fig. 2.36b).

Double Pulse Square Wave Voltammetry (DPSWV) is where both pulses are equal $t_1 = t_2$ and the pulse height ($\Delta E = E_2 - E_1$) is opposite from the scan direction (Fig. 2.36c). Because of its analogy with the potential-time program applied in Square Wave Voltammetry, it is referred to as Double Pulse Square Wave Voltammetry. *Differential Multi Pulse Voltammetry (DMPV)* is as a variant of DDPV where the initial conditions are not recovered during the experiment (Fig. 2.36d). Thus, the pulse length (t_p) is much shorter than the period between pulses (t_1), $t_1/t_p = 50\text{--}100$.

Differential Normal Multi Pulse Voltammetry (DNMPV) is the multi-pulse variant of the DMPV technique such that the duration of the period between pulses and the duration of the pulses are similar: $t_1 \approx t_p$ (Fig. 2.36e). Last, *Square Wave Voltammetry* can be considered as a particular situation of DNMPV where the length of both pulses are equal ($t_1 = t_p$) and the sign of the pulse height (ΔE) is opposite from the scan direction (Fig. 2.36f).

2.9 Other Voltammetric Techniques: Square Wave Voltammetry

The square wave voltammetric waveform consists of a square wave superimposed on a staircase, as shown in Fig. 2.37. The currents at the end of the forward and reverse pulses are both registered as a function of staircase potential. The difference between them, the net current, is larger than either of its two component parts in the region of the peak which is centred on the half-wave potential. Capacitative contributions can be effectively discriminated against before they die away, since, over a small potential range between forward and reverse pulses, the capacitance is constant and is thus annulled by subtraction. In this way the pulses can be shorter than in DPV and the square wave frequency can be higher. Instead of the effective sweep rates of $1\text{--}10 \text{ mVs}^{-1}$ of DPV, scan rates of 1 Vs^{-1} can be employed.

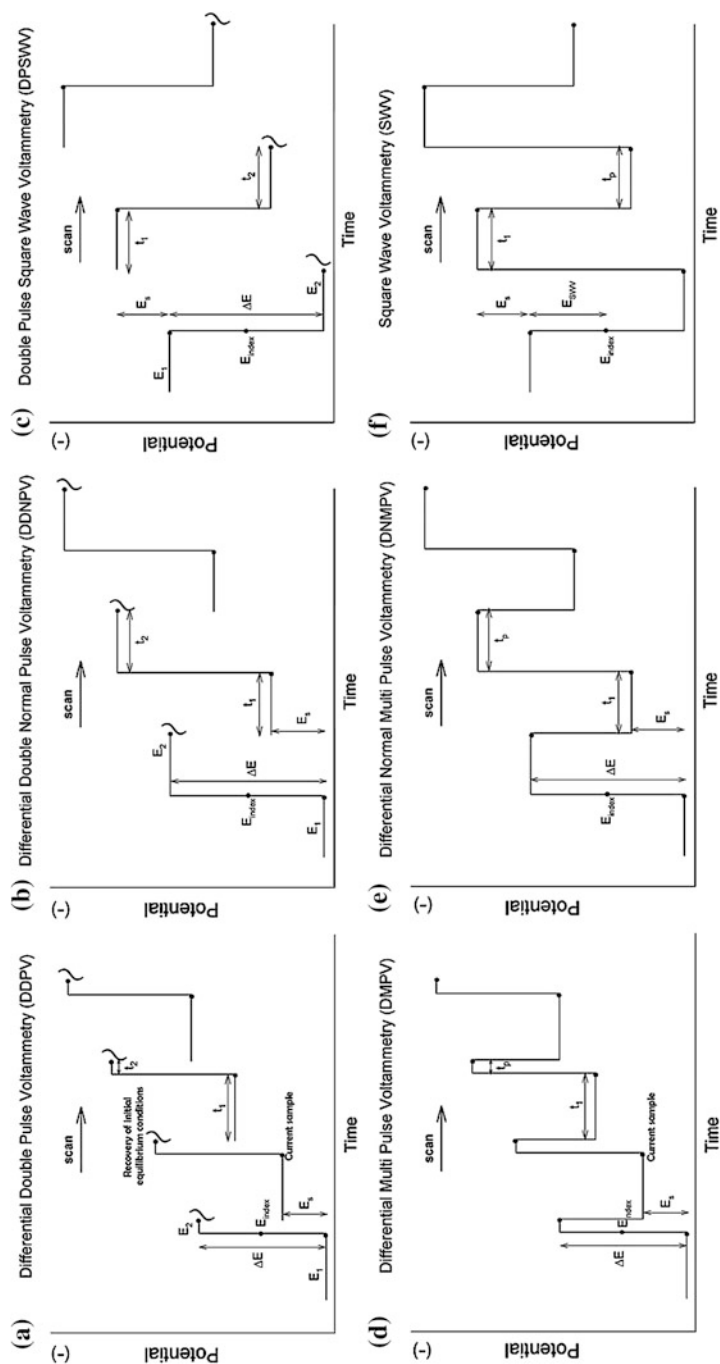


Fig. 2.36 Potential-time programs of the differential pulse techniques considered. Reproduced from Ref. [20] with permission from Elsevier

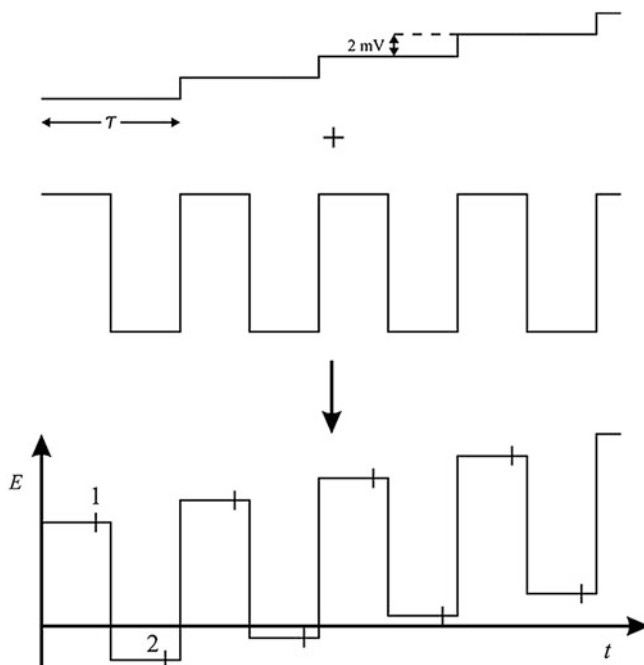


Fig. 2.37 Square wave voltammetry: waveform showing the summation of a staircase and a square wave

Detection limits of *ca.* 10^{-8} M or lower are readily achievable under optimum conditions. The advantages over cyclic voltammetry are as follows: faster scan rates are possible (faster reactions can be studied), higher sensitivity (lower concentrations can be used) and a higher dynamic range (a larger range of concentrations can be investigated). Usually in electrochemistry, solutions are vigorously degassed with, for example, nitrogen to remove oxygen which is electrochemically reduced and can interfere with the voltammetric measurement under investigation. A different way of greatly diminishing or eliminating the interference of oxygen, with no need for its removal, is by the use of the high frequencies employed in SWV. In fact, due to the irreversibility of oxygen reduction, the increase of its signal with frequency is small at high frequencies, and becomes negligible eventually, when compared with the response of the determinant [21] (Fig. 2.38).

2.10 Other Voltammetric Techniques: Stripping Voltammetry

Anodic Stripping Voltammetry (ASV) is an extremely sensitive electro-analytical technique that can determine trace quantities of certain metals at the parts-per-billion level. The first phase of an ASV experiment involves a pre-concentration

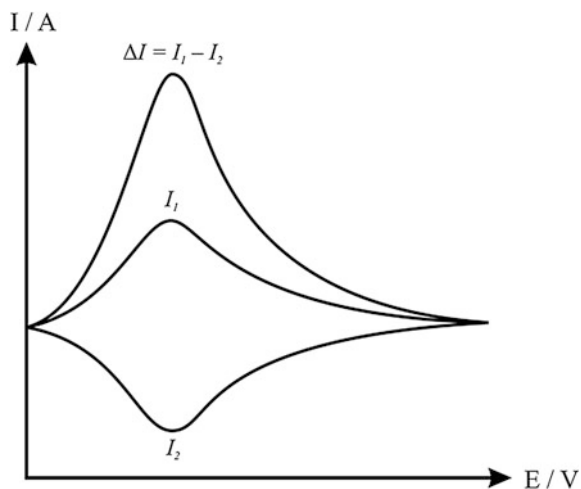


Fig. 2.38 Square wave voltammetry: voltammetric profile of current versus staircase potential. I_1 represents the forward and I_2 the reverse sweep where ΔI is the resultant voltammogram

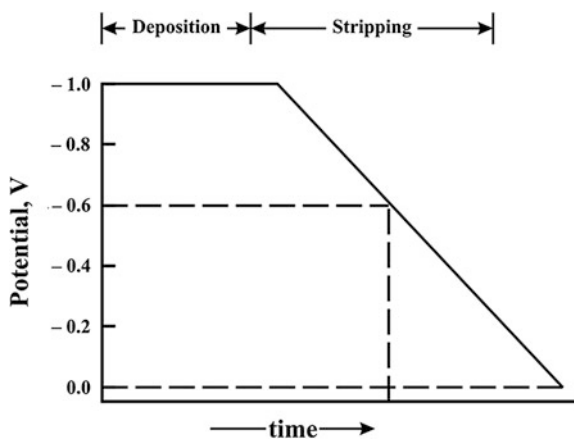
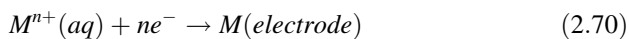


Fig. 2.39 A potential vs. time profile showing the stages in ASV

step, in which the analyte is deposited (i.e. in the case of metal analysis, reduced to its elemental form) at the working electrode by controlled potential electrolysis in a stirred solution at a suitable reduction potential as shown in Fig. 2.39. The process can be written as:



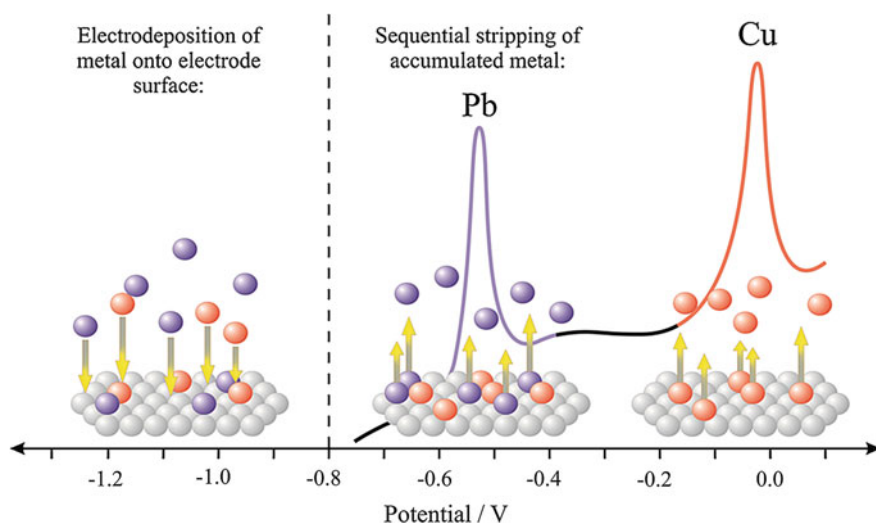


Fig. 2.40 A schematic representation of anodic stripping voltammetry showing the two key steps: electrodeposition and stripping

In the second phase, the potential of the working electrode is scanned so that the deposited metal is oxidised back to its ionic form, i.e. is anodically stripped from the electrode (see Fig. 2.39) by scanning the potential to a value where the following process occurs:

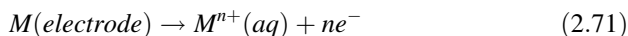
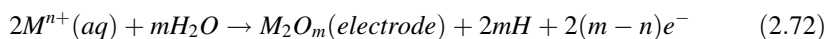


Figure 2.40 shows a schematic representation of this process for the case of lead and copper.

Additionally, as shown in Fig. 2.41, the potential—time profile can be used in ASV with a cleaning step (step A). This is usually applied in-between measurements to ensure that the deposited metal is fully stripped from the electrode surface so as to improve the reproducibility of the analytical measurement.

Figure 2.42 shows the response of a range of metals which occur at different stripping potentials allowing a multitude of metals to be readily analysed at once. The peak area and/or peak height of each stripping signal is proportional to concentration, allowing the voltammetric signal to be used analytically.

In addition to anodic stripping voltammetry there are also cathodic and adsorptive stripping voltammetry. In each case, similar to anodic stripping voltammetry, there is first a pre-conditioning step, which for cathodic stripping is either:



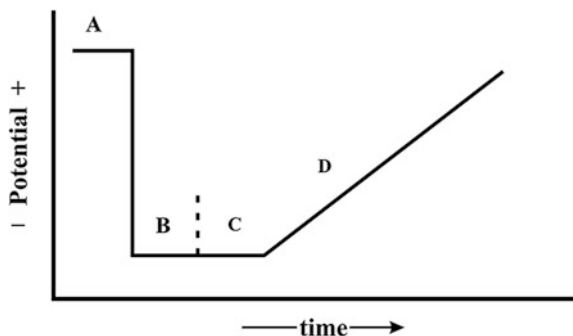
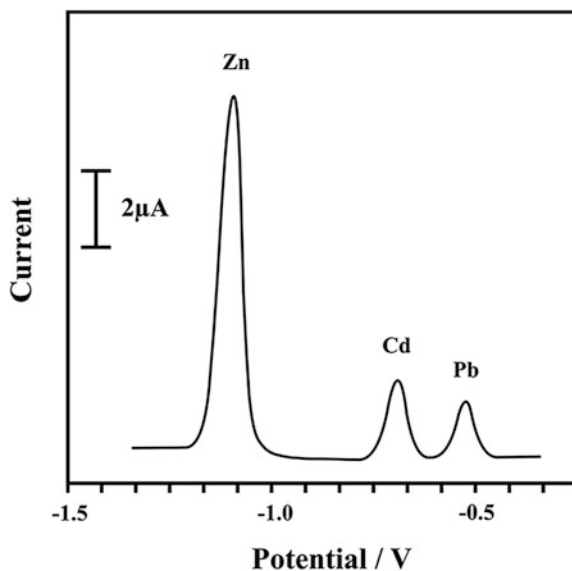
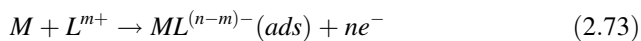


Fig. 2.41 A typical experimental potential—time profile used in ASV. Step A is the ‘Cleaning step’, B ‘electrodeposition’, C ‘Equilibration step’, D ‘Stripping step’

Fig. 2.42 Stripping voltammetry of zinc, cadmium and lead all in the same aqueous solution



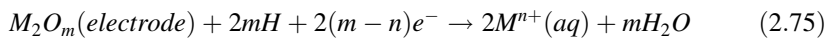
or



while for adsorptive stripping:



The corresponding stripping steps are for cathodic either:



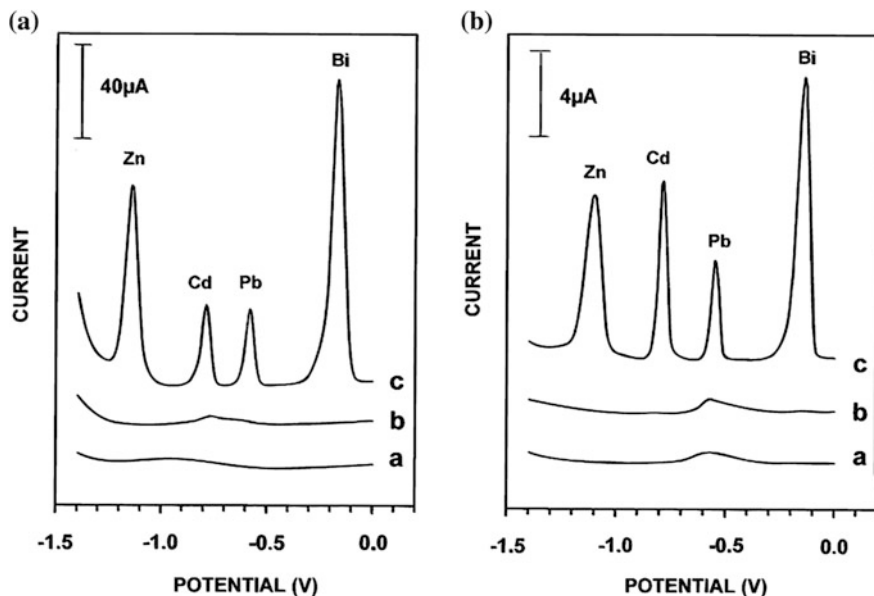
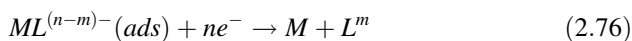


Fig. 2.43 Stripping voltammograms at glassy-carbon (a) and carbon-fiber (b) electrodes: *a* 0.1 M acetate buffer (pH 4.5); *b* as in (a) but after the addition of 50 $\mu\text{g/L}$ Cd(II), Pb(II), and Zn(II); *c* as in (b) but after the addition of 400 $\mu\text{g/L}$ Bi(III). Deposition for 120 s at -1.4 V; “cleaning” for 30 s at $+0.3$ V. Square-wave voltammetric stripping scan with a frequency of 20 Hz, potential step of 5 mV, and amplitude of 25 mV. Reproduced with permission from Ref. [32], copyright 2000 The American Chemical Society

or



while for adsorptive stripping:



To impart improvements in the voltammetric response, different electrode materials (and sizes to induce improvements in mass transport) can be used and traditionally mercury film and drop electrodes were utilised. Additionally, the use DPV and SWV can also provide benefits to reduce analytical limits of detection and improve sensitivities. However, due to the toxicity of mercury, considerable efforts have been devoted to the investigation of alternate electrode materials. Non-mercury electrodes, such as gold, carbon or iridium, have been explored but the overall performance of these alternatives has not approached that of mercury [22]. A verified alternative is the use of bismuth film electrodes (on various carbon

substrates) which offer high-quality stripping performance that compares favourably with that of mercury electrodes [22, 34].

Shown in Fig. 2.43 is the stripping performance of an in-situ modified bismuth-film electrode which also displays the corresponding control experiments (bare/unmodified electrode). No stripping signals are observed at the bare glassy-carbon (A(b)) and carbon-fibre (B(b)) electrodes for a sample containing 50 µg/L lead and cadmium. In contrast, adding 400 µg/L bismuth to the sample, and simultaneously depositing it along with the target metals, resulted in the appearance of sharp and undistorted stripping peaks for both analytes, as well as for bismuth (c).

The use of bismuth modified electrodes (through ex-situ and in-situ) modification has become a backbone of the electroanalytical community for a variety of target analytes [23].

2.11 Adsorption

In some instances, rather than having the analyte under investigation undergoing simply diffusional processes, the species of interest might adsorb onto the electrode surface and will give rise to different voltammetry. Figure 2.44 shows a typically voltammetric profile where a unique shape is observed. Since the adsorbed species does not have to diffuse to the electrode surface, the observed voltammogram is symmetrical.

The peak current can be related directly to the surface coverage (Γ) and potential scan rate for a reversible process:

$$I_p = \frac{n^2 F^2 \Gamma A v}{4RT} \quad (2.78)$$

with integration of the peak(s) shown in Fig. 2.44, allows the charge (Q) to be deduced, which is related to the surface coverage by the following expression:

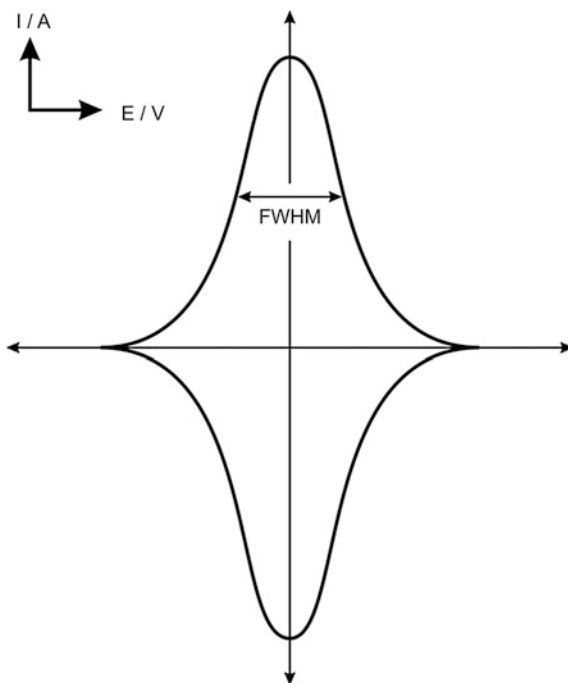
$$Q = nFA\Gamma \quad (2.79)$$

As shown in Fig. 2.44, the full width at half of the peak maximum height (FWHM) is given by:

$$FWHM = 3.53RT/nF \quad (2.80)$$

The diagnosis of an adsorbed species is to explore the effect of scan rate on the voltammetric response, which should yield a linear response for the case of I_p versus scan rate v . A practical example is shown in Fig. 2.45 where Hemoglobin (Hb)—Dimyristoyl phosphatidylcholine (DMPC) films are immobilised upon a BPPG surface. The modified electrode was then explored with the voltammetric response evident in Fig. 2.45a, with a plot of peak current against scan rate also

Fig. 2.44 Cyclic voltammetric response for the reversible reaction of an adsorbed species



provided. Near symmetric cyclic voltammetric profiles are observed with approximately equal reduction and oxidation peak heights, characteristic of *thin layer* electrochemical behaviour. As shown in Fig. 2.45, both cathodic and anodic peak potentials remain almost unchanged over the chosen scan rate range. A plot of \log_{10} (peak current) against \log_{10} (scan rate) was found to be linear with a slope of 0.98 (correlation coefficient of 0.999), which is very close to the expected theoretical slope of 1 for thin layer voltammetry as predicted by Eq. (2.78) [24].

In real situations, the adsorbed species may be weakly or strongly adsorbed. In these contexts, one usually refers to the reactants that are adsorbed, but four scenarios can be encountered, as elegantly shown in Fig. 2.46, each giving rise to unique and intriguing voltammetry.

Of note is that in the case of a strongly adsorbed reactant (Fig. 2.46d) there is a pre-peak before the solution phase voltammetric peak while in the case that the product is strongly adsorbed, the adsorption wave is seen following the solution phase peak (Fig. 2.46c). The effect of varying the voltammetric scan rate can be highly illuminating, as shown in Fig. 2.47 for the case of a strongly adsorbed product, where at slow scan rates (curve A) the adsorption wave is large relative to the first diffusional peak. As the scan rate is increased, the current of the adsorption peak decreases in magnitude while the diffusional peak current increases. At very high scan rates the adsorption wave is absent (curve D) [25].

There is also another scenario which can give rise to unique voltammetry. In the context of studying new materials, such as carbon nanotubes and indeed graphene

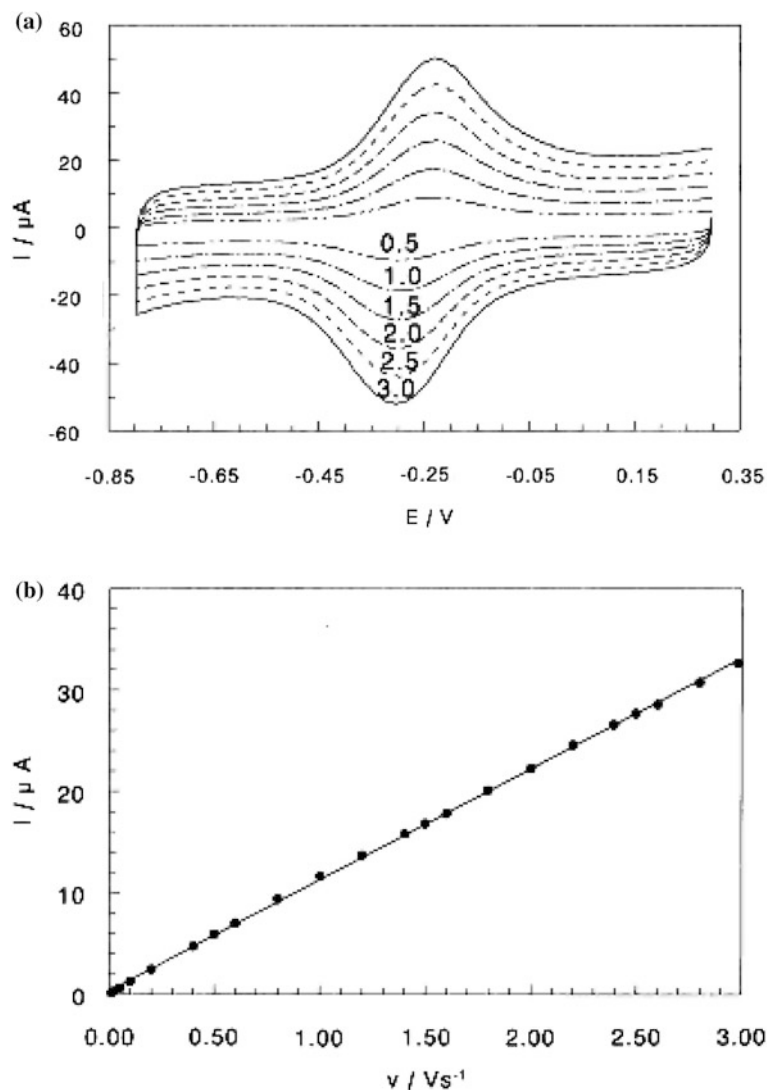
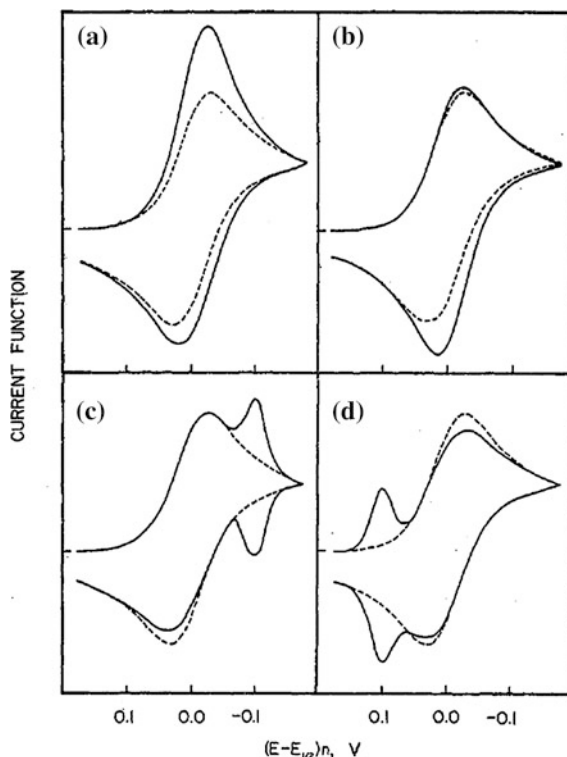


Fig. 2.45 Cyclic voltammograms **a** for Hb-DMPC films in pH 5.5 buffer at different scan rates (V s^{-1}); **b** influence of scan rate on reduction peak current. Reproduced from Ref. [24] with permission from Elsevier

which is the focus of this *handbook*, researchers usually disperse their chosen nanotubes into a non-aqueous solvent and put aliquots onto the working electrode of their choice. This modified surface is allowed to dry to enable the solvent to evaporate leaving the nanotubes immobilised upon the electrode surface, which is now ready to be electrochemically explored (the so called drop-coating method). This modified nanotube electrode surface is shown in Fig. 2.48. It has been shown

Fig. 2.46 Voltammetry with adsorption of reactants and products. **a** reactant adsorbed weakly; **b** product adsorbed weakly; **c** product adsorbed strongly; **d** reactant adsorbed strongly. *Dashed lines* are for response in the absence of adsorption. Reproduced with permission from Ref. [25], copyright 1967 The American Chemical Society



that the nanotube modified electrode exhibits a porous surface where ‘pockets’ of the electroactive species are trapped in-between multiple layers of nanotubes and the trapped species act akin to that of a *thin layer* cell [26]. The porous nanotube layer has a large surface area and the electrode is thought to be in contact with a finite, ‘thin-layer’ of solution (the species is trapped within the nanotube structure). In this case a mixture of diffusional regimes exists.

Figure 2.49 shows the voltammetry that will be observed as more nanotube material is immobilised upon the electrode surface, where there is an apparent improvement in the voltammetric peak height and a reduction in the potentials to lower values. Such a response has been assumed to be due to the electro-catalytic nature of the nanotubes themselves rather than a simple change in mass transport.

As thin-layer dominates, the ΔE_P changes from diffusional to that of thin-layer such that the peak-to-peak separation decreases giving the misleading impression that a material with fast electron transfer properties is giving rise to the response and hence misinterpretation can arise. Care also needs to be taken when adsorbing species are being explored as this will also give rise to thin layer type voltammetry [27]. Indeed the distinction between thin-layer diffusion and adsorption effects is not easy to make, especially in cases where the adsorption is rapidly reversible. Where there is slow adsorption (and desorption) kinetics, the presence or absence

Fig. 2.47 Voltammetric response at scan rates of 1 (A), 25 (B) 625 (C) and 2500 (D) Vs^{-1} for a product strongly adsorbed. Reproduced with permission from Ref. [25], copyright 1967 The American Chemical Society

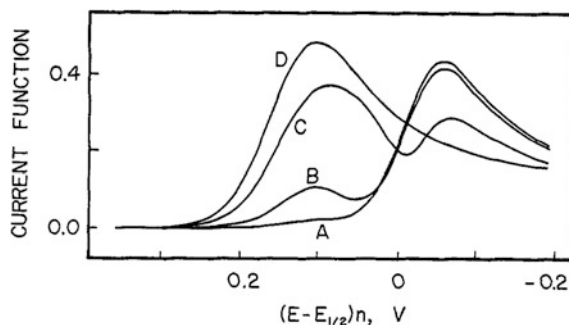


Fig. 2.48 Schematic representation of the two types of diffusion that contribute to the observed current at a highly porous CNT modified electrode. Reproduced from Ref. [26] with permission from Elsevier

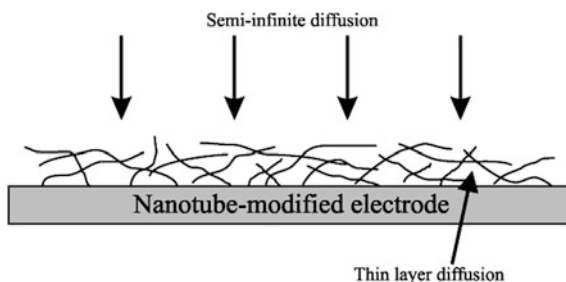
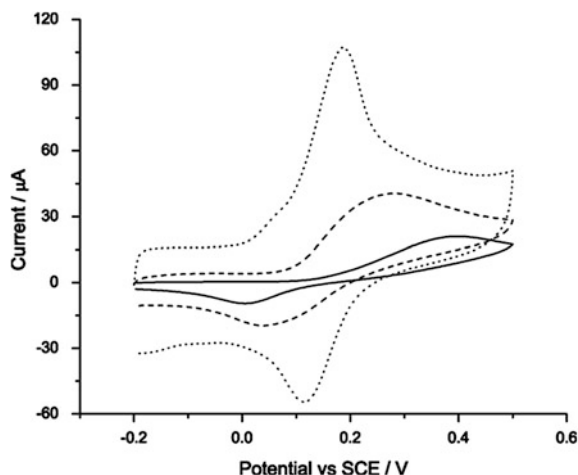


Fig. 2.49 Overlaid voltammograms recorded at 100 mVs^{-1} of 1 mM dopamine at a glassy carbon electrode modified with 0 μg (solid line), 0.4 μg (dashed line) and 2.0 μg (dotted line) MWCNTs. Reproduced from Ref. [26] with permission from Elsevier



of “memory effects” can be useful. If it is possible to transfer the electrode, after exposure to the target solution, to a fresh electrolyte containing no analyte, then adsorption effects can be inferred if voltammetric signals are retained or if signals increase steadily over a period of time [27].

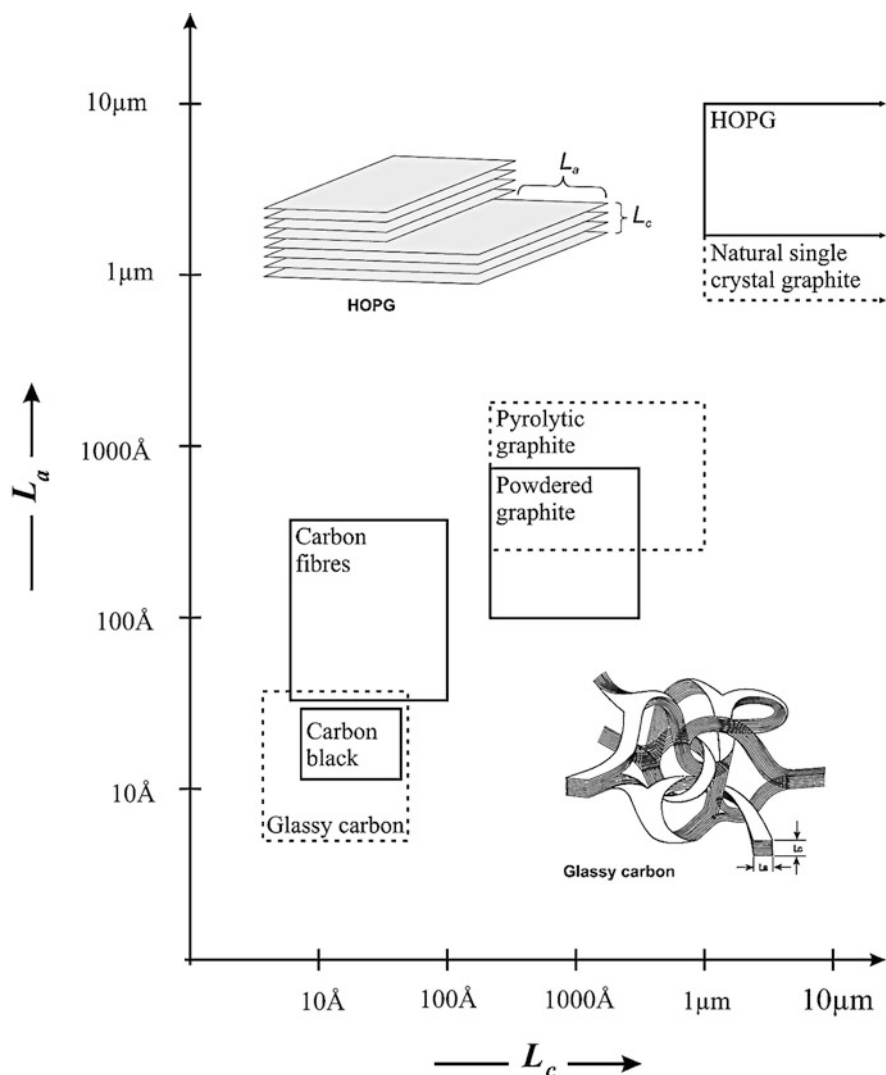


Fig. 2.50 The approximate ranges of L_a and L_c values for various sp^2 carbon materials. Note, there is large variation of L_a and L_c with sample history and thus the values shown should be considered representative, yet approximate. A schematic representation of the L_a and L_c microcrystalline characteristics of HOPG and glassy carbon is also shown

The above chapter is designed to give novices an insight into interfacial electrochemistry which can be used in interpret data presented in later chapters. Readers are directed to the following texts for further information on electrochemistry [6, 28].

2.12 Electrode Materials

There are a whole host of commercially available working electrodes which utilise a large variety of graphite products, such as amorphous carbon, glassy carbon, carbon black, carbon fibres, powdered graphite, pyrolytic graphite (PG) and highly ordered pyrolytic graphite (HOPG), each with different chemical and physical properties. The key structural factor that leads to such an assortment of different materials is the average graphite micro crystallites size (also known as the lateral grain size), L_a , which is effectively the average size of the hexagonal lattices that make up the macro structure. In principle, this can range from being infinitely large, as in the case of a macro single crystal of graphite, to the size of a benzene molecule; approximately 3 Å. In practice, the smallest L_a values are found in amorphous carbon, glassy carbon and carbon black and can be as low as 10 Å. Carbon fibres and pyrolytic graphite are intermediates in the range, with L_a values of *ca.* 100 Å and 1000 Å respectively. The assortment of materials are compared in Fig. 2.50 which reveals that the largest graphite monocrystals are found in high quality (ZYA and SPI 1 grade) HOPG, which can be 1–10 µm in size.

Regions where individual graphite monocrystals meet each other (i.e. grain boundaries) are poorly defined and when exposed result in surface defects. In the case of pyrolytic graphite, the individual graphite crystallites lie along the same axis making it possible to obtain carbon surfaces with significantly less defects. This is especially true for HOPG where the large lateral grain size can result in a well-defined surface with values of defect coverage as low as 0.2 % [29].

In Chap. 3 we consider the electrochemistry of graphene and the attempts made to understand this unique material.

References

1. T.J. Davies, C.E. Banks, R.G. Compton, *J. Solid State Electrochem.* **9**, 797–808 (2005)
2. H. Matsuda, Y. Ayabe, *Z. Elektrochem.* **59**, 494–503 (1955)
3. R.S. Nicholson, *Anal. Chem.* **37**, 1351–1355 (1965)
4. R.J. Klingler, J.K. Kochi, *J. Phys. Chem.* **85**, 1731–1741 (1981)
5. I. Lavagnini, R. Antiochia, F. Magno, *Electroanalysis* **16**, 505–506 (2004)
6. A.J. Bard, L.R. Faulkner, *Electrochemical Methods: Fundamentals and Applications*, 2nd edn. (Wiley, New York, 2001)
7. K. Stulik, C. Amatore, K. Holub, V. Marecek, W. Kutner, *Pure Appl. Chem.* **72**, 1483–1492 (2000)
8. A.C. Testa, W.H. Reinmuth, *Anal. Chem.* **33**, 1320–1324 (1961)
9. J.-A. Ni, H.-X. Ju, H.-Y. Chen, D. Leech, *Anal. Chim. Acta* **378**, 151–157 (1999)
10. R.G. Compton, C.E. Banks, *Understanding Voltammetry* (World Scientific, Singapore, 2007)
11. V.S. Vasantha, S.-M. Chen, *Electrochim. Acta* **52**, 665–674 (2006)
12. D. Shoup, A. Szabo, *J. Electroanal. Chem. Interfacial Electrochem.* **140**, 237–245 (1982)
13. M.Y. Abyaneh, *J. Electroanal. Chem.* **530**, 82–88 (2002)
14. M.Y. Abyaneh, M. Fleischmann, *J. Electroanal. Chem.* **530**, 89–95 (2002)
15. M.Y. Abyaneh, *J. Electroanal. Chem.* **530**, 96–104 (2002)

16. R.L. Deutscher, S. Fletcher, J. Electroanal. Chem. Interfacial Electrochem. **239**, 17–54 (1988)
17. R.L. Deutscher, S. Fletcher, J. Electroanal. Chem. Interfacial Electrochem. **277**, 1–18 (1990)
18. C.R. Wilke, P. Chang, Am. Inst. Chem. Eng. J. **1**, 264–270 (1955)
19. S. Shahrokhian, E. Asadian, Electrochim. Acta **55**, 666–672 (2010)
20. A. Molina, E. Laborda, F. Martínez-Ortiz, D.F. Bradley, D.J. Schiffrin, R.G. Compton, J. Electroanal. Chem. **659**, 12–24 (2011)
21. A.A. Barros, J.A. Rodrigues, P.J. Almeida, P.G. Rodrigues, A.G. Fogg, Anal. Chim. Acta **385**, 315–323 (1999)
22. J. Wang, J. Lu, U.A. Kirgoz, S.B. Hocevar, B. Ogorevc, Anal. Chim. Acta **434**, 29–34 (2001)
23. I. Švancara, C. Prior, S.B. Hocevar, J. Wang, Electroanalysis **22**, 1405–1420 (2010)
24. J. Yang, N. Hu, Bioelectrochem. Bioenerg. **48**, 117–127 (1999)
25. R.H. Wopschall, I. Shain, Anal. Chem. **39**, 1514–1527 (1967)
26. I. Streeter, G. G. Wildgoose, L. Shao, R. G. Compton, Sens. Actuators, B **133**, 462–466 (2008)
27. M. C. Henstridge, E. J. F. Dickinson, M. Aslanoglu, C. Batchelor-McAuley, R. G. Compton, Sens. Actuators, B **145**, 417–427 (2010)
28. J. Wang, *Analytical Electrochemistry*, 2nd edn. (Wiley-VCH, New York, 2000)
29. C. E. Banks, T. J. Davies, G. G. Wildgoose, R. G. Compton, Chem. Commun. 2005, 829–841
30. A.K. Yagati, T. Lee, J. Min, J.-W. Choi, Colloids Surf. B **92**, 161–167 (2012)
31. Y. Wang, E.I. Rogers, R.G. Compton, J. Electroanal. Chem. **648**, 15–19 (2010)
32. X. Cai, G. Rivas, P.A.M. Farias, H. Shiraishi, J. Wang, M. Fojta, E. Paleček, Bioelectrochem. Bioenerg. **40**, 41–47 (1996)
33. J. Wang, J. Lu, S.B. Hocevar, P.A.M. Farias, Anal. Chem. **72**, 3218–3222 (2000)
34. J. Tomeš, Collect. Czech. Chem. Commun. **9**, 12–21 (1937)

The Handbook of Graphene Electrochemistry

Brownson, D.A.C.; Banks, C.E.

2014, XII, 201 p. 126 illus., 40 illus. in color., Hardcover

ISBN: 978-1-4471-6427-2